AGU PUBLICATIONS

Tectonics

RESEARCH ARTICLE
10.1002/2016TC004283

Key Points:
- First zircon (U-Th)/He ages in the Marrakech High Atlas reveal a full development of a Mesozoic rift
- zHe ages evince Middle Jurassic to Early Cretaceous kilometer-scale postrift exhumation in the Marrakech High Atlas
- Late Cretaceous initiation of Atlas compression-driven exhumation evidenced by zHe data, with minimum values of total shortening of 17-21%

Supporting Information:
- Supporting Information S1
- Table S1

Correspondence to:
M. Domènech,
mireia.geologa@gmail.com

Citation:
Domènech, M., A. Teixell, and D. F. Stockli (2016), Magnitude of rift-related burial and orogenic contraction in the Marrakech High Atlas revealed by zircon (U-Th)/He thermochronology and thermal modeling, *Tectonics*, *35*, 2609–2635, doi:10.1002/2016TC004283.

Received 21 JUN 2016
Accepted 12 OCT 2016
Accepted article online 18 OCT 2016
Published online 19 NOV 2016

Magnitude of rift-related burial and orogenic contraction in the Marrakech High Atlas revealed by zircon (U-Th)/He thermochronology and thermal modeling

Mireia Domènech[1,2], Antonio Teixell[1], and Daniel F. Stockli[3]

[1]Departament de Geologia, Universitat Autònoma de Barcelona, Barcelona, Spain, [2]Now at División de Geociencias Aplicadas, Instituto Potosino de Investigación Científica y Tecnológica, San Luis Potosí, Mexico, [3]Department of Geological Sciences, Jackson School of Geosciences, University of Texas at Austin, Austin, Texas, USA

Abstract The Atlas of Morocco is a continental rift developed during the Triassic-Jurassic and moderately inverted during the Cenozoic. The High Atlas south of Marrakech, with exposures of basement and Triassic early synrift deposits, has been viewed as a high during the Mesozoic rifting. First zircon (U-Th)/He ages and thermal models obtained from 42 samples in the Marrakech High Atlas following two NNW-SSE transects across the mountain belt reveal that in contrast to previous models, the Triassic-Jurassic rift was well developed in the Marrakech High Atlas (with more than 4.5–6 km of rift-related deposits). Middle Jurassic-Early Cretaceous zHe cooling ages obtained indicate that rift-related subsidence in the Marrakech High Atlas finished in the Middle Jurassic and was followed by a period of exhumation where 2–3 km of rock were eroded. Thermal models from zHe data provide the first thermochronologic clue for a Late Cretaceous initiation of the Atlas compression-driven exhumation in the inner parts of the Marrakech High Atlas. The Triassic-Jurassic basin reconstruction assisted by thermochronology highlights a key role of inherited basement anisotropy in rift orientation and evolution, and on its subsequent inversion. Comparison of present-day and restored sections to the rifting stage aided by thermochronology suggests minimum values of total orogenic shortening in the Marrakech High Atlas of 13 to 14 km (21 to 17%), with exhumation of 1 to more than 5 km of rocks. Similar zHe ages on both sides of the Tizi n'Test fault evince minor vertical movements along the fault during the Atlas orogeny.

1. Introduction

The Atlas Mountains of Morocco are an intraplate orogen that formed during the Cenozoic in response to the Eurasia-Africa convergence. The Atlas orogen developed by the tectonic inversion with moderate shortening values of the aborted Mesozoic Atlas rift system, which was linked with the Atlantic and Tethys opening and formed in Triassic and Jurassic times [*Choubert and Faure-Muret*, 1962; *Mattauer et al*., 1977; *Frizon de Lamotte et al*., 2000; *Gomez et al*., 2000; *Piqué et al*., 2002; *Teixell et al*., 2003; *Arboleya et al*., 2004]. The High Atlas south of Marrakech (i.e., the Marrakech High Atlas or MHA), where this study is focused, is the region located between the Western and Central High Atlas (Figure 1). The geology of the MHA is dominated by basement and early synrift Triassic deposits. While numerous studies have investigated the evolution of the area during the Mesozoic rifting and Cenozoic orogeny, several aspects remain unresolved and/or controversial, such as the spatial extent and the magnitude of rift development in the area, as thick Jurassic carbonates and shales that outcrop in the Western and Central and Eastern High Atlas are largely absent in the MHA. Most studies have attributed this absence to modest amounts of Triassic-Jurassic rifting and representing a paleohigh or an area of limited subsidence (i.e., the West Moroccan Arch) that separated the Atlantic rift (to the west) from the Tethys rift (to the east) [*Choubert and Faure-Muret*, 1962; *Du Dresnay*, 1971; *Michard*, 1976; *Laville and Piqué*, 1991; *Stets*, 1992; *Jabour et al*., 2004; *Laville et al*., 2004; *El Arabi*, 2007; *Frizon de Lamotte et al*., 2008, 2009].

In contrast, some authors have recently suggested, on the basis of apatite fission track and (U-Th)/He ages, that the absence of Mesozoic rocks in the MHA could have been caused by vertical movements and exhumation either in Middle Jurassic-Early Cretaceous times, linked to E-W shortening [*Bertotti and Gouiza*, 2012], or in Cenozoic times, linked to the Atlas orogeny [*Missenard et al*., 2008; *Balestrieri et al*., 2009]. However, burial

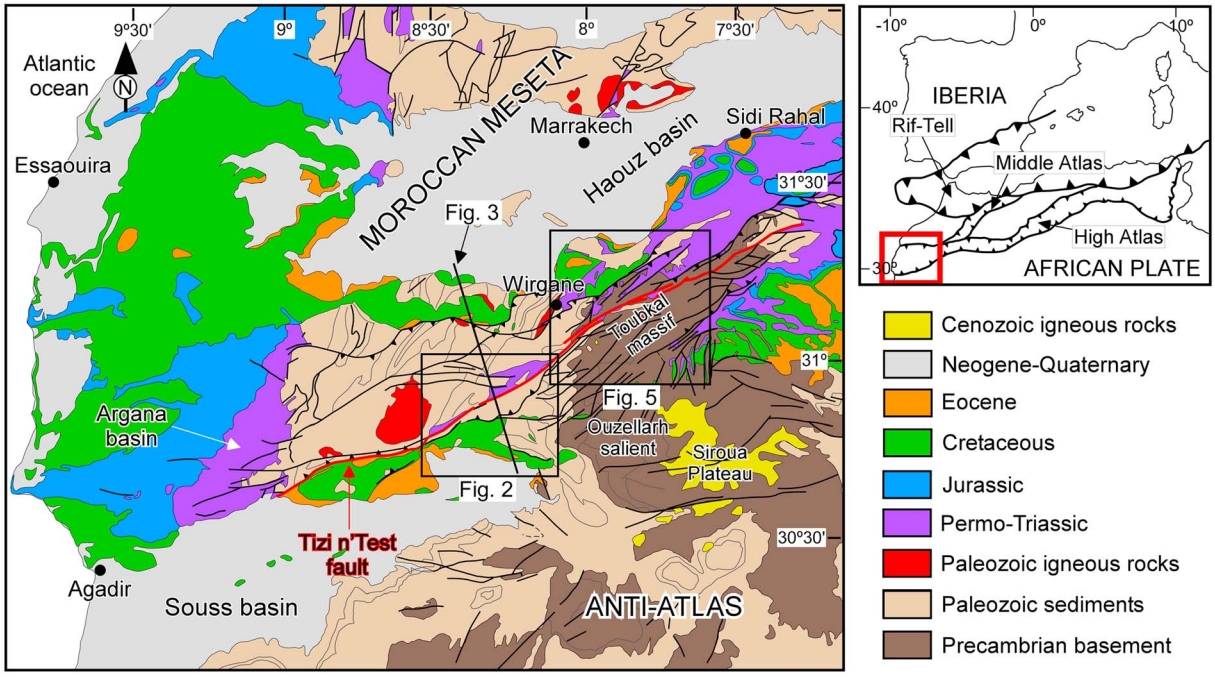

Figure 1. Geologic map synthesis of the Western and Marrakech High Atlas (modified from *Hollard* [1985]). Black squares show the Tizi n'Test (west) and Ourika-Toubkal (east) areas were thermochronologic ages were obtained for this study.

and exhumation events in the MHA remain insufficiently constrained, since structural and sedimentological observations only shed light on Early Triassic rifting (pre-Carnian) [*Domènech et al*., 2015] and limited thermochronologic data from the inner parts of the mountain belt were reset and yield Tertiary ages, providing no information on the pre-Tertiary thermal evolution [*Missenard et al*., 2008; *Balestrieri et al*., 2009; *Ghorbal*, 2009; *Bertotti and Gouiza*, 2012]. Similarly, the timing and magnitude of Atlas shortening is also only poorly constrained in the MHA, due to the scarcity of preserved synorogenic sediments and fault cutoffs of major thrusts. One of the major structural elements of the MHA is the so-called Tizi n'Test fault (Figure 1), a major and controversial fault zone interpreted either with strike-slip or dip-slip kinematics during Mesozoic extension and/or the Cenozoic compression [*Mattauer et al*., 1972, 1977; *Proust et al*., 1977; *Jenny*, 1983; *Binot et al*., 1986; *Froitzheim et al*., 1988; *Laville and Piqué*, 1991; *Amrhar*, 2002; *Qarbous et al*., 2003, 2008; *Laville et al*., 2004; *Delcaillau et al*., 2011]. More recently, however, this fault zone has been reinterpreted as a Triassic normal fault with only limited reactivation and movement during the Atlas orogeny [*Domènech et al*., 2015].

Zircon (U-Th)/He (zHe) thermochronometry with a higher closure temperature (~180°C) than the apatite (U-Th)/He (aHe) and apatite fission track (aFT) dating offers the potential to quantify thermal histories and burial and exhumation events obscured by subsequent thermal events and inaccessible to aFT and aHe dating. This study presents new zHe ages and thermal models from a set of 42 samples collected in the MHA along two NNW-SSE transects across the Atlas mountain belt. The integration of the zHe data and detailed crustal-scale structural analysis of the area [*Domènech et al*., 2015] allows for the reconstruction of the tectonic and thermal evolution of the MHA from Mesozoic times to the present. The interpretation of the zHe ages and thermal models demonstrate that the MHA experienced fully developed Triassic-Jurassic rifting followed by a period of exhumation in Middle Jurassic to Early Cretaceous. Furthermore, the data constrain the initiation of Atlas orogenic-driven exhumation as Late Cretaceous in age and illustrate that the MHA experienced moderate values of orogenic shortening.

2. Geologic Setting

The MHA is distinguished by an axial zone, characterized by basement and Permo-Triassic synrift deposits, and foothills composed of Cretaceous to Cenozoic postrift to syninversion deposits unconformably overlying basement or Triassic rocks (Figure 1). The basement shows two distinct tectonic domains, dominated by

Pan-African and Variscan orogenic imprint, respectively. In the area NW of the MHA, belonging to the Moroccan Meseta domain (Figure 1), basement is formed by Paleozoic rocks strongly affected by the Variscan orogeny and little overprint by subsequent deformation events. The area to the SE, belonging to the Anti-Atlas domain (Figure 1), is composed of Precambrian crystalline basement (onlaped by Paleozoic sedimentary rocks), with a dominant Pan-African structural grain and only a little Variscan and younger tectonic overprint [*Choubert and Faure-Muret*, 1962; *Mattauer et al*., 1972; *Froitzheim et al*., 1988; *Pique and Michard*, 1989; *Hoepffner et al*., 2005; *Michard et al*., 2010]. The boundary between both lithologic and rheologic domains is loosely defined but roughly follows the southern border of the High Atlas mountain belt. In the MHA such boundary deflects, bordering to the north the Precambrian massif of the Ouzellarh salient and being partially identified in the Tizi n'Test fault [*Choubert*, 1952; *Pique and Michard*, 1989; *Ouanaimi and Petit*, 1992; *Michard et al*., 2010] (Figure 1).

Early Mesozoic Atlas rifting is manifested in the MHA as a narrow and segmented NE-SW oriented rift with a complex system of horsts and grabens bounded by normal faults that formed during the Middle to earliest Late Triassic times [*Domènech et al*., 2015]. The preserved Triassic synrift strata consist of red beds with occasional evaporite layers, capped by basalt flows belonging to the Central Atlantic Magmatic province (CAMP) [*Bertrand and Prioton*, 1975; *Mattis*, 1977; *Biron and Courtinat*, 1982; *Manspeizer*, 1982; *Beauchamp*, 1988; *Knight et al*., 2004]. Jurassic deposits are absent in the MHA.

The inversion of the High Atlas rift occurred mainly during the Cenozoic [*Mattauer et al*., 1977; *Frizon de Lamotte et al*., 2000; *Piqué et al*., 2002; *Teixell et al*., 2003; *Tesón et al*., 2010]. The earliest evidence for the onset of contractional deformation and folding comes from angular and progressive unconformities in Late Cretaceous to Eocene inliers within the High Atlas [*Laville et al*., 1977; *Froitzheim et al*., 1988; *Herbig*, 1988; *Tesón*, 2009; *Michard et al*., 2011]. However, folding appears to have been very limited and the existence of regionally extensive subtabular limestone deposits of Paleocene to mid-Eocene age is not consistent with the development of an Atlas flexural, orogenic foreland basin system [*Herbig and Trappe*, 1994; *Tesón and Teixell*, 2008; *Tesón*, 2009]. Furthermore, some of the Eocene structures have been recently reinterpreted as caused by salt diapirism [*Michard et al*., 2011].

As for the main episodes of contractional deformation in the Atlas, different phases of Oligocene to Pleistocene shortening have been proposed on the basis of syntectonic sediments, although there are marked discrepancies in interpretation among different authors [*Laville et al*., 1977; *Fraissinet et al*., 1988; *Görler et al*., 1988; *Jacobshagen et al*., 1988; *Harfi et al*., 1996; *Frizon de Lamotte et al*., 2000; *Tesón et al*., 2010]. Field observations combined with magnetostratigraphy in the Sub-Atlas thrust belt north of the Ouarzazate basin, along the southern margin of the Central High Atlas, show that main thrust activity in the external fold-and-thrust belt begun during the Oligocene or early Miocene and extended up to recent times [*Fraissinet et al*., 1988; *Morel et al*., 2000; *Tesón and Teixell*, 2008; *Tesón et al*., 2010]. The initiation of orogenic deformation in the High Atlas hinterland was placed in the mid-Eocene on the basis of the occurrence of Lutetian sandstones and microconglomerates in the Sub-Atlas, interpreted as first foreland basin deposits [*Harfi et al*., 1996; *Frizon de Lamotte et al*., 2000; *Tesón and Teixell*, 2008; *Tesón et al*., 2010]. The chronology of deformation in the internal parts of the High Atlas is only poorly constrained, but Oligocene-Miocene aFT ages from the MHA [*Missenard et al*., 2008; *Balestrieri et al*., 2009; *Ghorbal*, 2009] and thermal modeling of aFT ages from the Central High Atlas [*Barbero et al*., 2007] indicate a Neogene age for the main phase of thrusting.

Rift inversion in the Central High Atlas is characterized by thick-skinned deformation with the reactivation of former normal faults and formation of new contractional structures [*Froitzheim et al*., 1988; *Frizon de Lamotte et al*., 2000; *Teixell et al*., 2003]. The MHA shows similar structural anatomy [*Missenard et al*., 2007; *Domènech et al*., 2015] with the distinct difference that the reactivation of former normal faults was only minor [*Domènech et al*., 2015]. Thin-skinned deformation is concentrated in narrow thrust belts along the orogen margins [*Laville et al*., 1977; *Beauchamp et al*., 1999; *Frizon de Lamotte et al*., 2000; *Teixell et al*., 2003; *Missenard et al*., 2007; *Tesón and Teixell*, 2008; *Domènech et al*., 2015]. Total orogenic shortening from the restoration of post-Variscan strata in the Central High Atlas has been estimated as 24% to 18% from east to west, respectively [*Teixell et al*., 2003]. In the MHA, cross sections and fault displacements are more difficult to quantify due to the sparse preservation of post-Variscan stratigraphic markers and shortening estimates range from <3 km (4%) [*Missenard et al*., 2007] to >13 km (~16%) [*Domènech et al*., 2015]. The moderate amounts of shortening of the High Atlas are in stark contrast to the mean topography of the mountain range.

This discrepancy, coupled with gravity data, has led studies to suggest that the system is isostatically undercompensated at crustal levels and to invoke mantle-related uplift in the Atlas region [*Van Den Bosch*, 1971; *Makris et al*., 1995; *Teixell et al*., 2003; *Ayarza et al*., 2005]. The onset of dynamic uplift has been dated at ~15 or 5 Ma on the basis of the post-Miocene magmatism and various paleoelevation markers [*Teixell et al*., 2005; *Missenard et al*., 2006; *Babault et al*., 2008]. Potential field and 3-D modeling of the lithosphere-asthenosphere boundary have defined the existence of a NE trending, 400 km wide asthenosphere upwelling zone beneath the Moroccan Atlas [*Missenard et al*., 2006; *Fullea et al*., 2007]. However, the MHA is thought to lie outside the main thinned lithosphere domain despite containing the highest summits of the Atlas Mountains (e.g., the Toubkal massif; Figure 1).

3. Zircon (U-Th)/He Methodology

(U-Th)/He dating is a thermochronometric technique widely employed in tectonic studies, which makes use of the radioactive decay of alpha particles from ^{238}U, ^{235}U, ^{232}Th, and ^{147}Sm leading to the production of ^{4}He nuclei (i.e., α particles). Retention of radiogenic ^{4}He in zircon is controlled by thermally activated volume diffusion [*Zeitler et al*., 1987; *Lippolt et al*., 1994; *Wolf et al*., 1996; *Farley*, 2000]. Laboratory experiments and empirical borehole studies indicate that He is not retained at temperatures above 200°C and is mostly retained below ~130°C, defining the zircon He partial retention zone (zPRZ) [*Reiners et al*., 2002, 2004; *Reiners*, 2005; *Wolfe and Stockli*, 2010]. The nominal closure temperature for the He thermochronometer (Tc) in zircon is estimated at ~180°C [*Reiners*, 2005; *Wolfe and Stockli*, 2010]. However, the He diffusivity in zircon is affected by diffusion domain (grain) size, lattice anisotropy, and the radiation damage [*Reiners et al*., 2002, 2004; *Cherniak et al*., 2009; *Guenthner et al*., 2013; *Ketcham et al*., 2013] (see discussion in Text S1 in the supporting information). In addition to diffusive controls on He loss, alpha particles (He nucleus) can be ejected from the outer ~20 μm of the grain, requiring a morphometric alpha-ejection correction (Ft) [*Farley et al*., 1996; *Farley*, 2000; *Ketcham et al*., 2011]. All samples were processed and all zircon (U-Th)/He analysis were carried out at the UTChron facilities at the University of Texas, following analytical procedures of *Wolfe and Stockli* [2010]. Complete procedures are detailed in the supporting information. All reported ages are alpha-ejection corrected (F_T), and errors are standard errors (~8%, 2σ) on the basis of reproducibility of the Fish Canyon Tuff standard.

A suite of 42 samples was collected in the MHA in two different areas. In the west, zHe ages were obtained from the Tizi n'Test Triassic basin and its adjacent southern margin and in the east, zHe ages were obtained in the Ourika-Tizi n'Tacht Triassic basin and basement of the Toubkal Massif area (Figure 1). Detailed results are given in Tables 1, 2, and S1. Some samples were collected and grouped in elevation profiles and interpreted as vertical profiles, assuming that samples have belonged to the same structural block since cooling below the zHe closure temperature (and hence, the vertical offset between samples was invariant over time). In addition, while some elevation profiles cover as much as 4 km of horizontal distance, we assumed that the lateral cooling and effects of topographic dynamics and isotherm perturbations in the zHe system are negligible in light of the high closure temperature (~180°C). All inverse thermal modeling of zHe ages has been carried out with the QTQt software [*Gallagher*, 2012], which uses the Bayesian transdimensional Markov Chain Monte Carlo (MCMC) approach described by *Gallagher et al*. [2009]. A detailed description of the QTQt software and MCMC approach is presented in Text S2.

4. Zircon (U-Th)/He Results

4.1. Tizi n'Test Area

In the Tizi n'Test area, 19 samples were collected following a NNW-SSE transect across the Triassic basin, the adjacent Paleozoic basement, and the Lower Cretaceous (the Infracenomanian Unit) (Figure 2). Samples are grouped in four profiles (Figures 2 and 3). The zHe ages obtained for each profile are described in following sections.

4.1.1. N'fis, Abarnous, and Tama'rout Elevation Profiles

Six samples (MiHe-39T, MiHe-40T, MiHe-46T to MiHe-49T, and MiHe-63T) were collected in the Triassic rocks preserved in the Tizi n'Test basin (the N'fis elevation profile in Figures 2 and 3) between 1370 m and 2061 m of altitude. Sample MiHe-49T was collected in the F3 conglomeratic unit, attributed to the Lower to Middle Triassic (the overlying F4 unit was dated as Anisian [*El Arabi et al*., 2006]), and the other samples were

Table 1. Zircon (U-Th)/He Data From the Tizi n'Test Area

Grain Lab N°	Corrected age ±8% (Ma)	Uncorrected age (Ma)	Elevation (m)	Grain Lab N°	Corrected age ±8% (Ma)	Uncorrected age (Ma)	Elevation (m)
N'fis profile				zMiHe-41T-5	111.17 ± 8.89	80.48	
zMiHe-39T-1	132.24 ± 10.58	107.45	1716	zMiHe-41T-6	134.34 ± 10.75	95.40	
zMiHe-39T-2	439.07 ± 35.13	361.75			*35.96%*		
zMiHe-39T-3	113.38 ± 9.07	92.88		zMiHe-43T-1	156.63 ± 12.53	125.15	2367
zMiHe-39T-4	214.56 ± 17.16	170.20		zMiHe-43T-2	130.92 ± 10.47	98.83	
zMiHe-39T-5	208.91 ± 16.71	169.94		zMiHe-43T-3	121.84 ± 9.75	96.44	
zMiHe-39T-6	122.67 ± 9.81	96.90			*25.49%*		
	158.77%			zMiHe-45T-1	74.21 ± 5.94	58.41	2234
zMiHe-40T-1	151.49 ± 12.12	115.82	1584	zMiHe-45T-2	154.74 ± 12.38	121.07	
zMiHe-40T-2	183.91 ± 14.71	138.51		zMiHe-45T-3	110.38 ± 8.83	81.09	
zMiHe-40T-3	151.81 ± 12.15	123.81		zMiHe-45T-4	188.77 ± 15.10	143.63	
zMiHe-40T-4	194.85 ± 15.59	157.04		zMiHe-45T-5	135.49 ± 10.84	105.37	
zMiHe-40T-5	173.61 ± 13.89	131.40		zMiHe-45T-6	127.07 ± 10.17	104.59	
zMiHe-40T-6	175.94 ± 14.08	137.81			*86.93%*		
	25.22%			zMiHe-56T-1	106.60 ± 8.53	80.83	1685
zMiHe-46T-1	183.65 ± 14.69	138.09	1784	zMiHe-56T-2	84.73 ± 6.78	58.92	
zMiHe-46T-2	113.34 ± 9.07	87.76		zMiHe-56T-3	160.88 ± 12.87	118.96	
zMiHe-46T-3	200.33 ± 16.03	159.48		zMiHe-56T-4	66.48 ± 5.32	46.31	
zMiHe-46T-4	195.97 ± 15.68	143.87		zMiHe-56T-5	116.89 ± 9.35	85.73	
zMiHe-46T-5	189.39 ± 15.15	146.11		zMiHe-56T-6	125.39 ± 10.03	85.23	
zMiHe-46T-6	170.76 ± 13.66	127.58			*85.70%*		
	49.55%			zMiHe-57T-2	164.29 ± 13.14	132.11	1588
zMiHe-48T-1	90.03 ± 7.20	70.44	1876	zMiHe-57T-4	208.75 ± 16.70	166.83	
zMiHe-48T-2	166.82 ± 13.35	134.48		zMiHe-57T-5	222.18 ± 17.77	170.68	
zMiHe-48T-3	133.72 ± 10.70	103.81			*29.18%*		
zMiHe-48T-4	316.92 ± 25.35	245.34		zMiHe-58T-1	214.53 ± 17.16	173.28	1989
zMiHe-48T-5	157.91 ± 12.63	121.60		zMiHe-58T-2	178.90 ± 14.31	141.23	
zMiHe-48T-6	373.07 ± 29.85	303.89		zMiHe-58T-3	150.99 ± 12.08	118.27	
	137.13%				*35.01%*		
zMiHe-49T-1	164.98 ± 13.20	126.50	2061	zMiHe-60T-3	161.21 ± 12.90	131.53	1842
zMiHe-49T-2	231.05 ± 18.48	187.15		zMiHe-60T-4	177.32 ± 14.19	137.68	
zMiHe-49T-3	206.65 ± 16.53	154.93		zMiHe-60T-6	171.50 ± 13.72	137.27	
zMiHe-49T-4	148.45 ± 11.88	114.92			*9.48%*		
zMiHe-49T-5	403.44 ± 32.28	325.48		*Al Mdad profile*			
zMiHe-49T-6	89.70 ± 7.18	68.10		zMiHe-50T-1	295.76 ± 23.66	220.96	797
	151.29%			zMiHe-50T-2	153.27 ± 12.26	122.38	
zMiHe-63T-1	149.83 ± 11.99	117.18	1371	zMiHe-50T-3	273.58 ± 21.89	219.11	
zMiHe-63T-2	145.04 ± 11.60	114.33		zMiHe-50T-4	351.95 ± 28.16	282.08	
zMiHe-63T-3	90.16 ± 7.21	68.65		zMiHe-50T-5	252.30 ± 20.18	193.19	
zMiHe-63T-4	103.63 ± 8.29	78.51		zMiHe-50T-6	207.92 ± 16.63	161.97	
zMiHe-63T-5	104.73 ± 8.38	80.86			*77.67%*		
zMiHe-63T-6	101.21 ± 8.10	74.66		zMiHe-54T-1	263.36 ± 21.07	194.71	855
	51.54%			zMiHe-54T-2	353.96 ± 28.32	259.84	
Abarnous and Tama'rout profiles				zMiHe-54T-3	272.73 ± 21.82	205.01	
zMiHe-36T-1	217.84 ± 17.43	174.38	2018	zMiHe-54T-5	290.53 ± 23.24	218.95	
zMiHe-36T-2	211.36 ± 16.91	156.36		zMiHe-54T-6	248.92 ± 19.91	197.31	
zMiHe-36T-3	217.80 ± 17.42	161.64			*36.74%*		
zMiHe-36T-4	239.12 ± 19.13	180.43		zMiHe-55T-1	252.31 ± 20.18	184.70	1297
zMiHe-36T-5	219.48 ± 17.56	162.85		zMiHe-55T-2	284.95 ± 22.80	219.26	
zMiHe-36T-6	218.70 ± 17.50	165.61		zMiHe-55T-3	256.77 ± 20.54	207.11	
	12.58%			zMiHe-55T-4	258.59 ± 20.69	204.12	
zMiHe-38T-1	255.65 ± 20.45	210.50	1806	zMiHe-55T-5	233.24 ± 18.66	179.58	
zMiHe-38T-2	142.26 ± 11.38	109.01		zMiHe-55T-6	286.07 ± 22.89	211.60	
zMiHe-38T-3	151.88 ± 12.15	117.55			*20.16%*		
zMiHe-38T-4	129.25 ± 10.34	102.30		zMiHe-61T-1	315.67 ± 25.25	249.21	1273
zMiHe-38T-5	153.94 ± 12.32	115.91		zMiHe-61T-2	261.02 ± 20.88	213.82	
zMiHe-38T-6	155.83 ± 12.47	124.23		zMiHe-61T-3	291.15 ± 23.29	241.49	
	76.69%			zMiHe-61T-5	237.99 ± 19.04	181.61	
zMiHe-41T-1	163.17 ± 13.05	125.59	2525	zMiHe-61T-6	317.09 ± 25.37	246.62	

Table 1. (continued)

Grain Lab N°	Corrected age ±8% (Ma)	Uncorrected age (Ma)	Elevation (m)	Grain Lab N°	Corrected age ±8% (Ma)	Uncorrected age (Ma)	Elevation (m)
zMiHe-41T-3	153.90 ± 12.31	116.08			*27.8%*		
zMiHe-41T-4	160.39 ± 12.83	125.10					

[a]The intrasample grain age dispersion (range of the ages divided by the mean, as used by *Brown et al.* [2013]) is shown in italics.

collected in the F5 sandstone unit, dated as Carnian [*Cousminer and Manspeizer*, 1976; *Biron and Courtinat*, 1982]. The zircons analyzed yield Ft-corrected ages ranging from 90.0 ± 7.2 Ma to 439.1 ± 35.1 Ma (Figure 4a; see details in Tables 1 and S1) with intrasample grain age dispersion (range of the ages divided by the mean [*Brown et al.*, 2013]) from 25.2% to 158.7%. Intrasample age dispersions in excess of the analytical error is commonly attributed to factors such as grain size, U and Th zonation, radiation damage, or age inheritance in detrital grains (see discussion in Text S1). As direct relationships between grain size, zonation, or radiation damage with intrasample dispersion are not observed, the fact that many zHe ages obtained from the Triassic sedimentary rocks are older than their depositional age indicates that these zHe ages were only partially or not reset and (partially) preserve their detrital age signature. Consequently, samples were only heated to temperatures of 130–150°C (lower portion of the zPRZ) after Triassic sedimentation. To deduce this, we make the assumption that the amount of zircon grains analyzed is representative of the whole detrital zircon population of the sample. The same assumption is made for the other Paleozoic-Cretaceous detrital rocks sampled in the Tizi n'Test area.

The zHe ages of the N'fis elevation profile do not exhibit any clear elevation dependence (Figure 4a). Although the potential existence of minor undetected faults and the coexistence of variably reset and non-reset zHe ages may influence the data scatter, the cluster pattern of Figure 4a suggests that samples were heated during burial and cooled rapidly through the zPRZ. Stratigraphic lower samples (collected at F3 and basal F5 Triassic units) are currently located at higher elevations than samples collected from stratigraphic higher positions (collected at the upper part of the F5 Triassic unit; Figure 4a) due to tilting that must have occurred in response to Neogene Atlas orogeny and after the samples cooled through the zPRZ (Figure 2) [*Domènech et al.*, 2015]. Using the constraints on the stratigraphic position of Triassic samples and of the thicknesses of different Triassic units, samples were projected into the section of Figure 3b both at their current elevation (black squares) and at their original stratigraphic position (grey squares). As the tilting of the Triassic units occurred after zHe resetting, the initial stratigraphic position of the samples (i.e., the initial vertical offset between samples) was used for the interpretation of these zHe ages.

The nine samples of the Abarnous and Tama'rout elevation profiles (MiHe-36T, MiHe-38T, MiHe-41T to MiHe-45T, and MiHe-56T to MiHe-60T) were collected south of the Tizi n'Test basin from Cambrian siliciclastic and volcanoclastic rocks [*Angoud et al.*, 2002] (Figures 2 and 3). The Abarnous and Tama'rout elevation profiles have 719 m and 401 m of elevation difference, respectively (Table 1 and Figures 4b and 4c). Samples are located in a structural block between the Tizi n'Test Triassic basin and the Cretaceous-Paleozoic samples of the Sub-Atlas Zone adjacent to the Souss basin (Figure 3). This block is bounded to the north by synrift normal faults belonging to the Tizi n'Test fault zone and to the south by the Tama'rout thrust (Figure 3b) [*Domènech et al.*, 2015]. The five samples of the Abarnous elevation profile yield corrected zHe ages from 74.2 ± 5.9 Ma to 255.7 ± 20.5 Ma (Table 1 and Figure 4b) with intrasample grain age dispersion from 12.6% to 86.9%. The four samples of the Tama'rout elevation profile yield corrected zHe ages from 66.5 ± 5.3 Ma to 222.2 ± 17.8 Ma (Table 1 and Figure 4c) with intrasample grain age dispersion that ranges from 9.5% to 85.7% (Table 1).

All the zHe ages from both profiles are younger than their corresponding depositional ages, indicating that the zHe ages were fully reset after deposition. The profiles show no elevation-dependent zHe ages suggesting that samples cooled rapidly through the zPRZ. The zHe ages show significant intrasample age dispersion that cannot be explained by grain size, radiation damage, or zonation, suggesting that the samples possibly resided in the zPRZ prior to fast cooling and might retain some variable age inheritance or kinetic differences.

The Triassic samples of the N'fis elevation profile and the Paleozoic samples of the Abarnous and Tama'rout elevation profiles exhibit similar zHe ages and hence likely shared a similar cooling history. Plotting the zHe

Table 2. Zircon (U-Th)/He Data From the Ourika-Toubkal Area[a]

Grain Lab N°	Corrected Age ±8% (Ma)	Uncorrected Age (Ma)	Elevation (m)	Grain Lab N°	Corrected Age ±8% (Ma)	Uncorrected Age (Ma)	Elevation (m)
Imlil profile				zMiHe-23-4	221.73 ± 17.74	174.13	
zMiHe-02-2	111.63 ± 8.93	91.84	1608		*36.07%*		
zMiHe-02-3	131.80 ± 10.54	107.57		zMiHe-24-1	132.42 ± 10.59	106.13	1989
	16.57%			zMiHe-24-2	121.30 ± 9.70	93.80	
zMiHe-03-1	123.18 ± 9.86	98.31	1982	zMiHe-24-3	185.39 ± 14.83	138.39	
zMiHe-03-2	110.02 ± 8.80	89.20			*43.79%*		
zMiHe-03-3	104.93 ± 8.39	82.50		zMiHe-25-1	199.87 ± 16.00	167.51	2221
	16.20%			zMiHe-25-2	215.57 ± 17.25	175.69	
zMiHe-04-1	127.70 ± 10.22	106.87	2241	zMiHe-25-3	199.51 ± 15.96	164.30	
zMiHe-04-4[b]	469.09 ± 37.53	395.44			*7.84%*		
zMiHe-04-3	85.69 ± 6.85	67.36		zMiHe-27-1	280.66 ± 22.45	230.27	1791
	39.37%			zMiHe-27-2	234.86 ± 18.79	181.34	
zMiHe-06-2[b]	178.90 ± 14.31	132.06	2587	zMiHe-27-3	286.35 ± 22.91	236.22	
zMiHe-06-3[b]	59.34 ± 4.75	41.51			*19.26%*		
	100.36%			*Ourika profile*			
zMiHe-08-1	249.69 ± 19.98	168.13	2994	zMiHe-28-1	35.03 ± 2.80	28.40	1494
zMiHe-08-2	43.73 ± 3.50	31.25		zMiHe-28-2	49.22 ± 3.94	38.96	
zMiHe-08-3	24.76 ± 1.98	16.92		zMiHe-28-3	45.21 ± 3.62	35.00	
	212.08%				*32.89%*		
Tizi n'Likemt profile				zMiHe-29-1	63.78 ± 5.10	50.54	1780
zMiHe-12-1	63.75 ± 5.10	51.19	3629	zMiHe-29-2	61.84 ± 4.95	49.52	
zMiHe-12-2[b]	708.74 ± 56.70	569.01		zMiHe-29-3	42.18 ± 3.37	32.80	
zMiHe-12-3	63.39 ± 5.07	48.91			*38.63%*		
	0.56%			zMiHe-30-1	46.40 ± 3.71	36.88	2038
zMiHe-15-1	52.13 ± 4.17	42.89	2998	zMiHe-30-2	56.80 ± 4.54	45.20	
zMiHe-15-2	47.98 ± 3.84	37.74		zMiHe-30-3	48.65 ± 3.89	40.19	
zMiHe-15-3	20.28 ± 1.62	17.03			*20.54%*		
	79.37%			zMiHe-31-1	66.07 ± 5.29	53.01	2204
zMiHe-17-1	135.32 ± 10.83	109.49	2559	zMiHe-31-2	76.52 ± 6.12	58.87	
zMiHe-17-2	98.44 ± 7.88	70.77		zMiHe-31-3	59.53 ± 4.76	49.07	
zMiHe-17-3	90.01 ± 7.20	66.93			*25.22%*		
	41.99%			zMiHe-32-1	67.04 ± 5.36	54.43	2401
Tizgui profile				zMiHe-32-2	52.59 ± 4.21	42.18	
zMiHe-19-1	322 ± 25.76	251.15	3198		*24.16%*		
zMiHe-19-2	305.74 ± 24.46	244.13		zMiHe-33-1	64.15 ± 5.13	52.51	2595
zMiHe-19-3	298.10 ± 23.85	233.51		zMiHe-33-2	92.12 ± 7.37	72.47	
	7.74%			zMiHe-33-3	54.14 ± 4.33	44.02	
zMiHe-20-1	273.72 ± 21.90	206.01	2831		*54.16%*		
zMiHe-20-3	131.64 ± 10.53	104.48		zMiHe-34-1	151.79 ± 12.14	124.72	2818
	70.10%			zMiHe-34-2	113.22 ± 9.06	87.52	
zMiHe-21-1	265.55 ± 21.24	197.71	2574	zMiHe-34-3	59.51 ± 4.76	47.17	
zMiHe-21-2	305.87 ± 24.47	229.99			*85.31%*		
zMiHe-21-3	188.50 ± 15.08	154.83		zMiHe-35-1	112.71 ± 9.02	91.65	3029
	46.33%			zMiHe-35-2	156.11 ± 12.49	128.43	
zMiHe-23-1	152.96 ± 12.24	112.79	2202	zMiHe-35-3	97.75 ± 7.82	79.50	
zMiHe-23-2	197.27 ± 15.78	154.05			*47.76%*		

[a]The intrasample grain age dispersion (range of the ages divided by the mean, as used by *Brown et al.* [2013]) is shown in italics.
[b]Grains that are not included in the interpretation (see supporting information for explanation).

ages of these three vertical profiles together shows that samples rapidly cooled through the zPRZ at an age of 154 ± 43 Ma (Figure 4e) (calculated using the BayesMixQt software [*Jasra et al.*, 2006], using a statistical Gaussian distribution; see Text S2 for details).

4.1.2. Al Mdad Samples

Four samples were collected in the southern foothills of the MHA (Sub-Atlas zone), separated from the Paleozoic and Triassic samples to the north by the Tama'rout thrust (Figure 3). Samples MiHe-50T, MiHe-55T, and MiHe-61T were collected from poorly sorted sandstone of the Infracenomanian Unit, while sample MiHe-54T was collected from an Early Cambrian sandstone [*Angoud et al.*, 2002] (Figures 2 and 3) at elevations of 797 m to 1297 m (Table 1). The Cambrian sample yielded corrected zHe ages ranging from

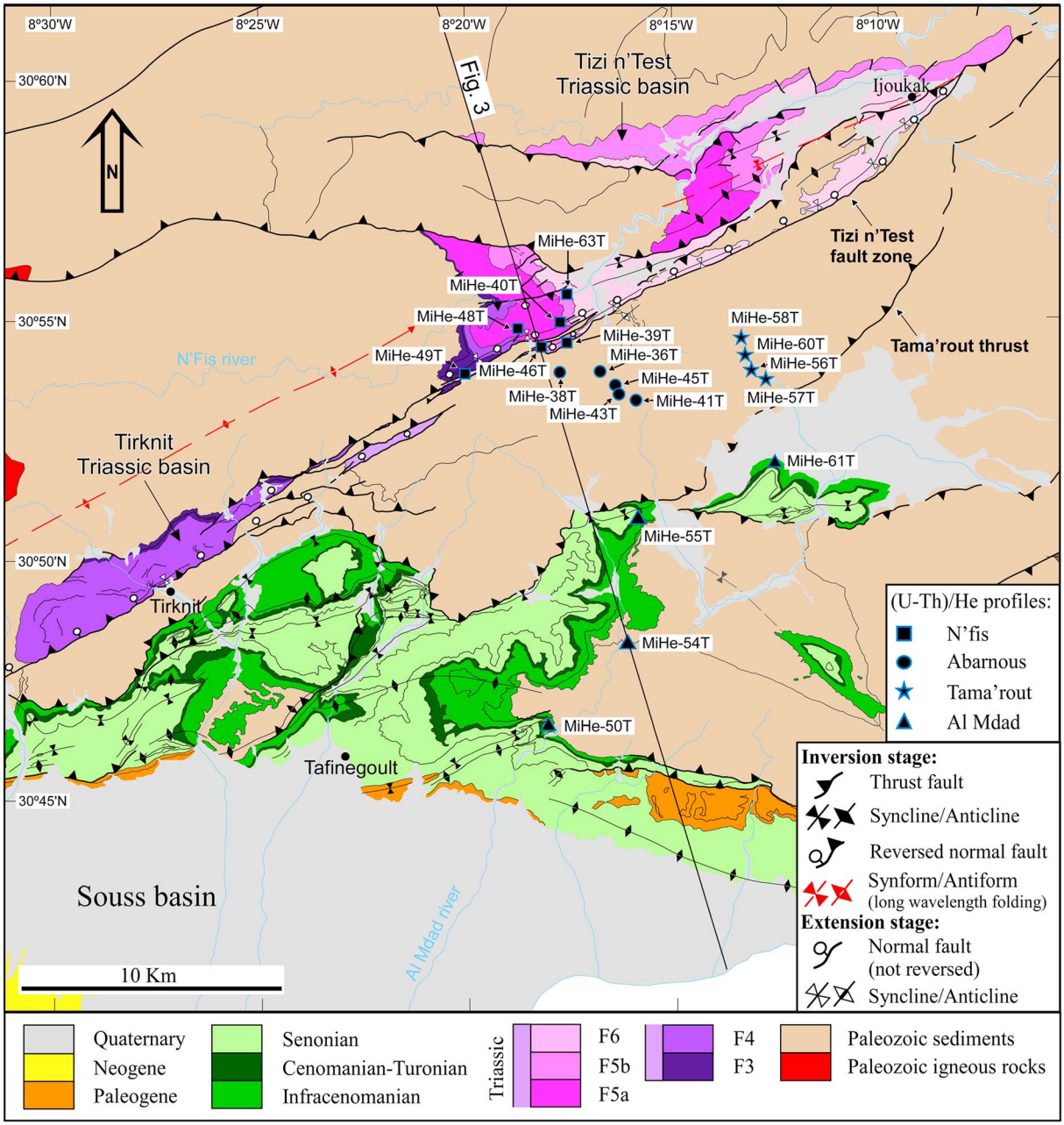

Figure 2. Geologic map of the Tizi n'Test area in the MHA (see location in Figure 1) showing the main structural elements and the location of samples analyzed in this work.

248.9 ± 19.9 Ma to 354.0 ± 28.3 Ma (Figure 4d). Therefore, the sample was heated and reset after its deposition, exhumed through the zPRZ in Carboniferous-Permian times, probably due to the Variscan orogeny and remained at temperatures below the zPRZ since then.

Samples of the Infracenomanian Unit yield corrected zHe ages from 153.9 ± 12.3 Ma to 352.0 ± 28.2 Ma (Table 1). All zHe ages are older than their depositional ages (Figure 4d), suggesting that they were likely not heated above 130°C after sedimentation. Seventy-seven percent of all detrital zHe ages are Carboniferous to Permian, similar to the zHe ages from the Cambrian sample, which implies a nearby Paleozoic or Precambrian source area where zHe ages were not reset in post-Paleozoic times. The remaining 23% of detrital zHe ages are Triassic-Jurassic, which could indicate a source area where zircon grains rapidly cooled during Triassic-Jurassic unroofing or that zircons are derived from the erosion of igneous rocks of that age.

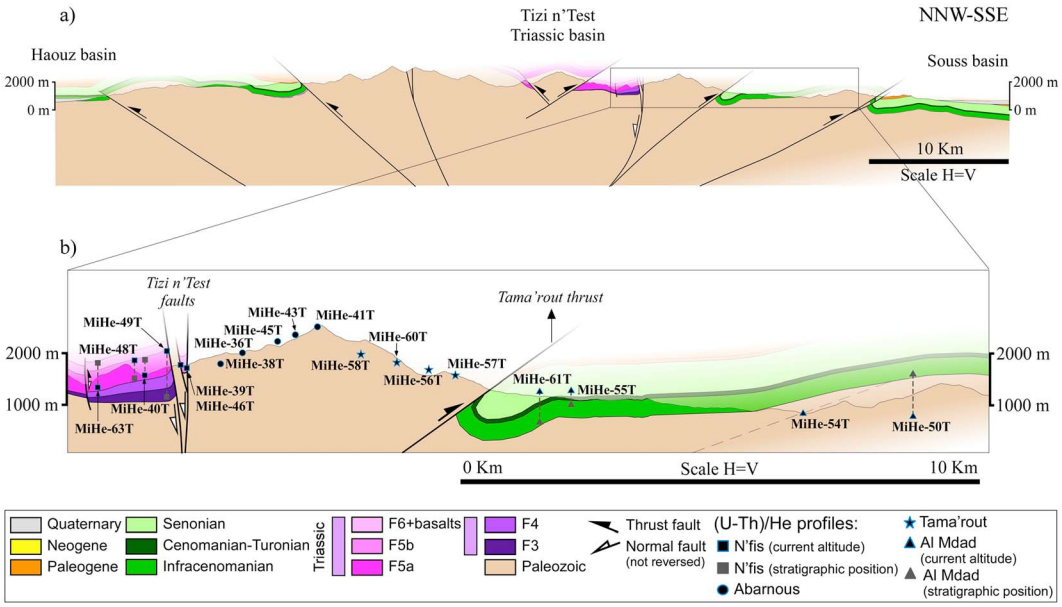

Figure 3. (a) General section of the MHA across the Tizi n'Test Triassic basin (see location in Figures 1 and 2) (modified from *Domènech et al.* [2015]). (b) Close-up of the Tizi n'Test basin and its margin with samples projected at their present altitude. In grey we show a projection following the stratigraphic position of the samples (see text for explanation).

4.2. Ourika-Toubkal Area

To the east of the MHA, in the Ourika-Toubkal area, 23 samples were collected from rhyolitic and granitic basement rocks of the Precambrian basement (Table 2), including four elevation profiles along two NNW-SSE transects (Figures 5 and 6).

4.2.1. Ourika Elevation Profile

A set of eight samples (MiHe-28 to MiHe-35) was collected from Neoproterozoic granitic rocks (Assarag Suite; U-Pb zircon age of 614–575 Ma [*Thomas et al.*, 2002]). The elevation profile has over ~1500 m of local relief. The eight samples yield corrected zHe ages from 35.0 ± 2.8 Ma to 156.1 ± 12.5 Ma (Table 2), which represent the youngest zHe ages obtained for the MHA. Samples from the Ourika profile are from both the Ourika river thalweg and hillslope (black squares in Figures 5 and 6b).

The Precambrian samples come from the southern margin of the Triassic Ourika rift basin (Figure 5) and likely resided at near-surface temperatures prior to Triassic rifting in the Ourika area. ZHe ages plotted define a positive age-elevation relationship (Figure 7a). The bottom samples show intrasample zHe age dispersion from 20.5% to 38.6%, while the two upper samples present intrasample dispersion from 47.8% to 85.3% (Table 2). The high intrasample age dispersion of the upper samples appears to indicate that they resided within the zPRZ and were not completely reset prior to exhumation.

Sample MiHe-29 was collected from south of the Ourika fault while others in the profile were collected north of it (Figures 5 and 6b). The Ourika fault, which continues for another ~25 km to the NE from the area represented in Figure 5, is regarded as part of the Tizi n'Test fault zone [e.g., *Proust et al.*, 1977] and based on structural criteria is interpreted as a normal fault active during the rifting stage, but not reactivated during Cenozoic shortening [*Domènech et al.*, 2015]. The coherent positive age-elevation relationship in the zHe ages (Figure 7a) implies that no major displacement occurred along the Ourika fault from Late Cretaceous times to the present. Previous aFT ages, ranging from 11.5 ± 0.6 Ma to 16.9 ± 0.7 Ma, also show no significant age differences across the Ourika fault and corroborate limited to no fault motion in the Cenozoic [*Missenard et al.*, 2008] (Figures 5 and 7a). Accordingly, samples of the Ourika elevation profile are considered to belong to the same structural block since zircon He closure, allowing for these zHe ages to be modeled together.

4.2.2. Imlil, Tizi n'Likemt, and Tizgui Elevation Profiles

Samples of the Imlil elevation profile (MiHe-02 to MiHe-08) were collected in the Ighighayene river valley in the vicinity of Imlil town and in the Toubkal massif between 1608 m and 2994 m (Table 2 and Figure 6a).

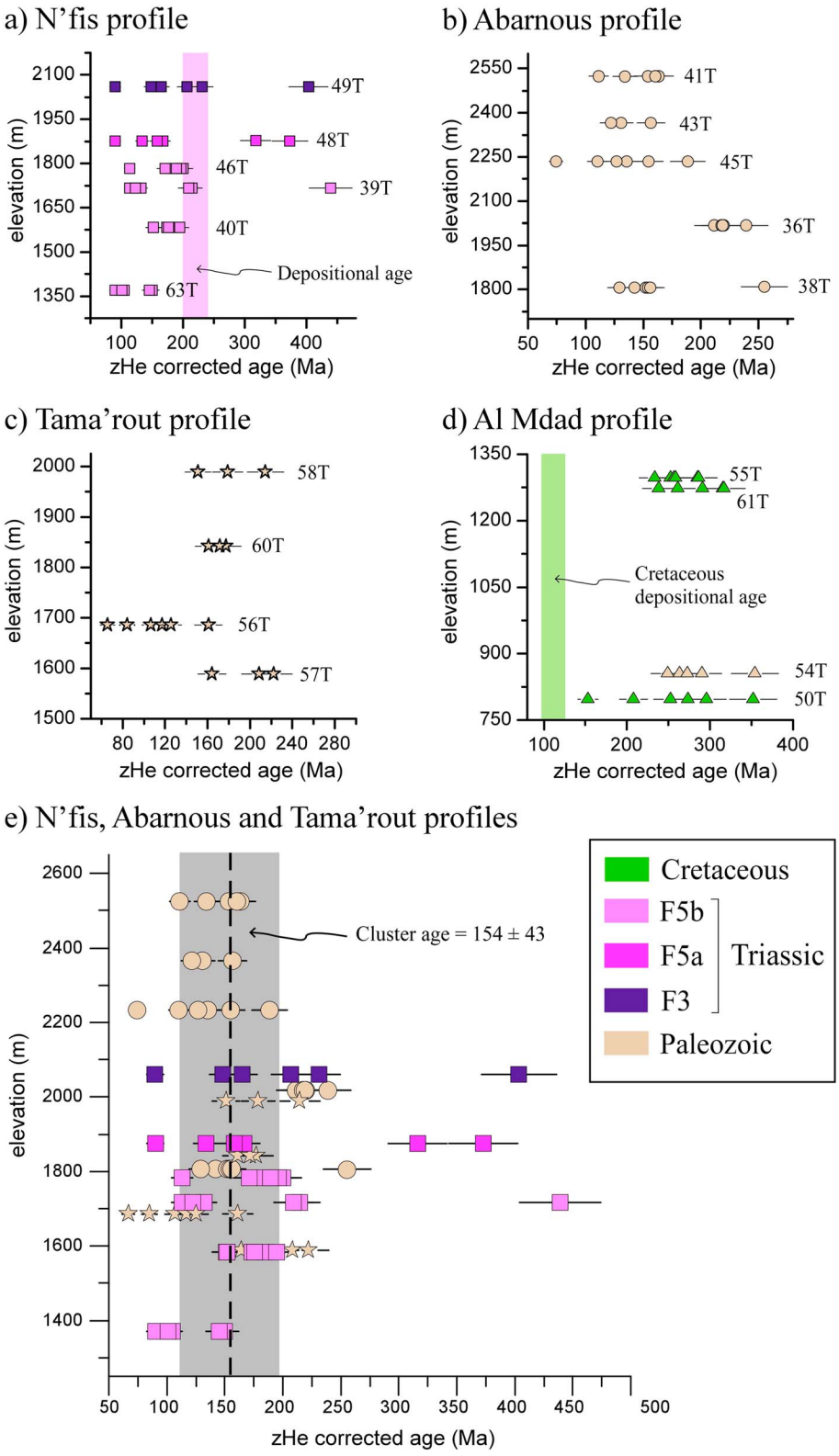

Figure 4. Age-elevation plots with 2σ error for the (a) N'fis, (b) Abarnous, (c) Tama'rout, and (d) Al Mdad profiles (see location in Figure 2). (e) Age-elevation plot with 2σ error for the N'fis, Abarnous, and Tama'rout profiles showing a cluster zHe age at 154 ± 43 Ma.

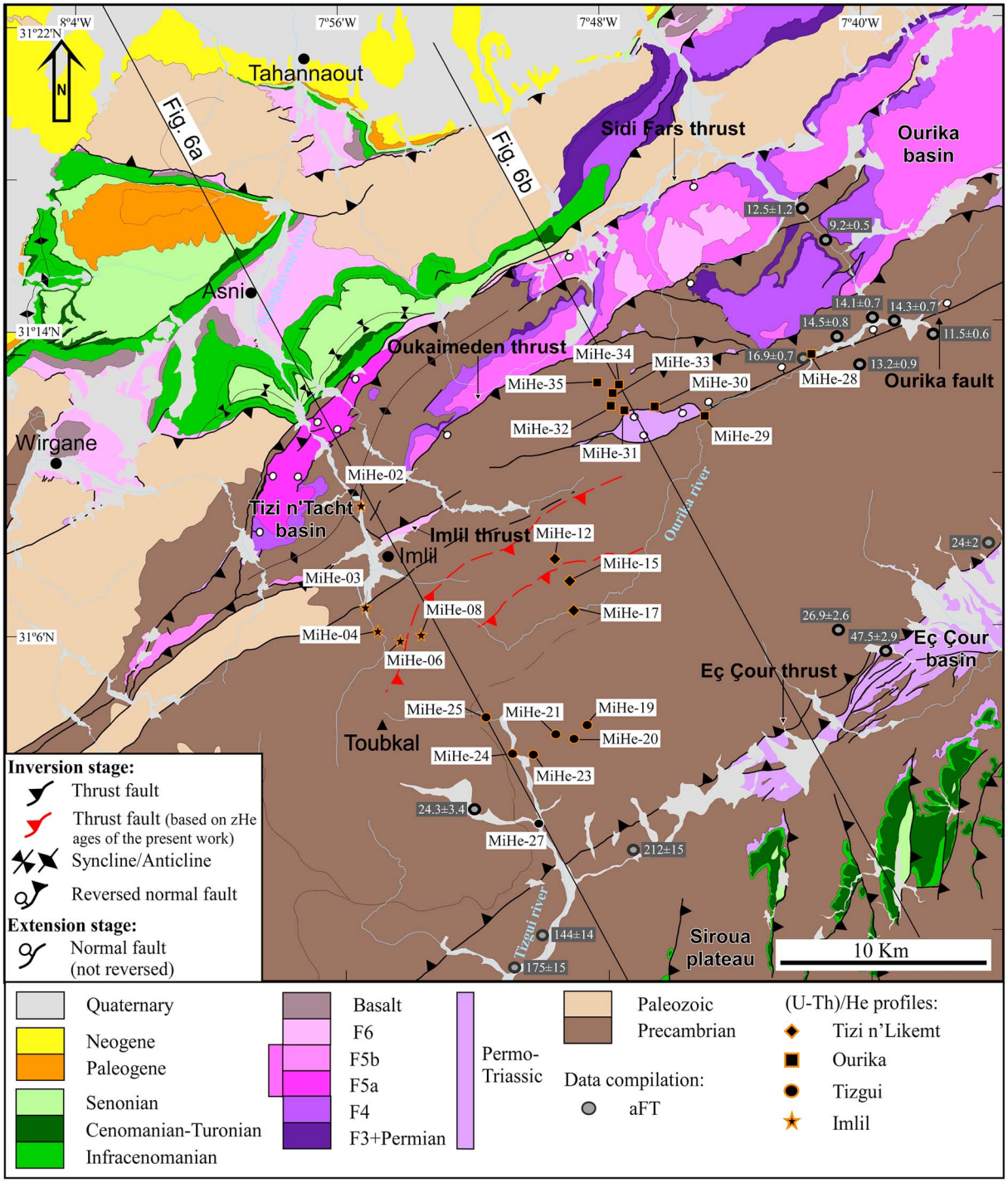

Figure 5. Geologic map of the Ourika-Toubkal area in the MHA (see location in Figure 1) showing the main structural elements and the location of samples of the four elevation profiles. The location of preexisting low-temperature data (aFT ages) is shown by grey circles [*Missenard et al.*, 2008; *Balestrieri et al.*, 2009].

Sample MiHe-02 was collected from a granite of the Assarag Suite ~300 m below the unconformity with Triassic deposits (F4 unit, Anisian in age [*El Arabi et al.*, 2006]) (Figures 5 and 6a). The other samples, MiHe-03 to MiHe-08, are 560–575 Ma rhyolites of the Ouarzazate Group [*Thomas et al.*, 2002].

The four samples suitable for interpretation from the Imlil vertical profile yielded corrected zHe ages from 24.8 ± 2.0 Ma to 249.7 ± 20.0 Ma. Intrasample grain age dispersion ranges from 16.2% to 212.1%. Sample

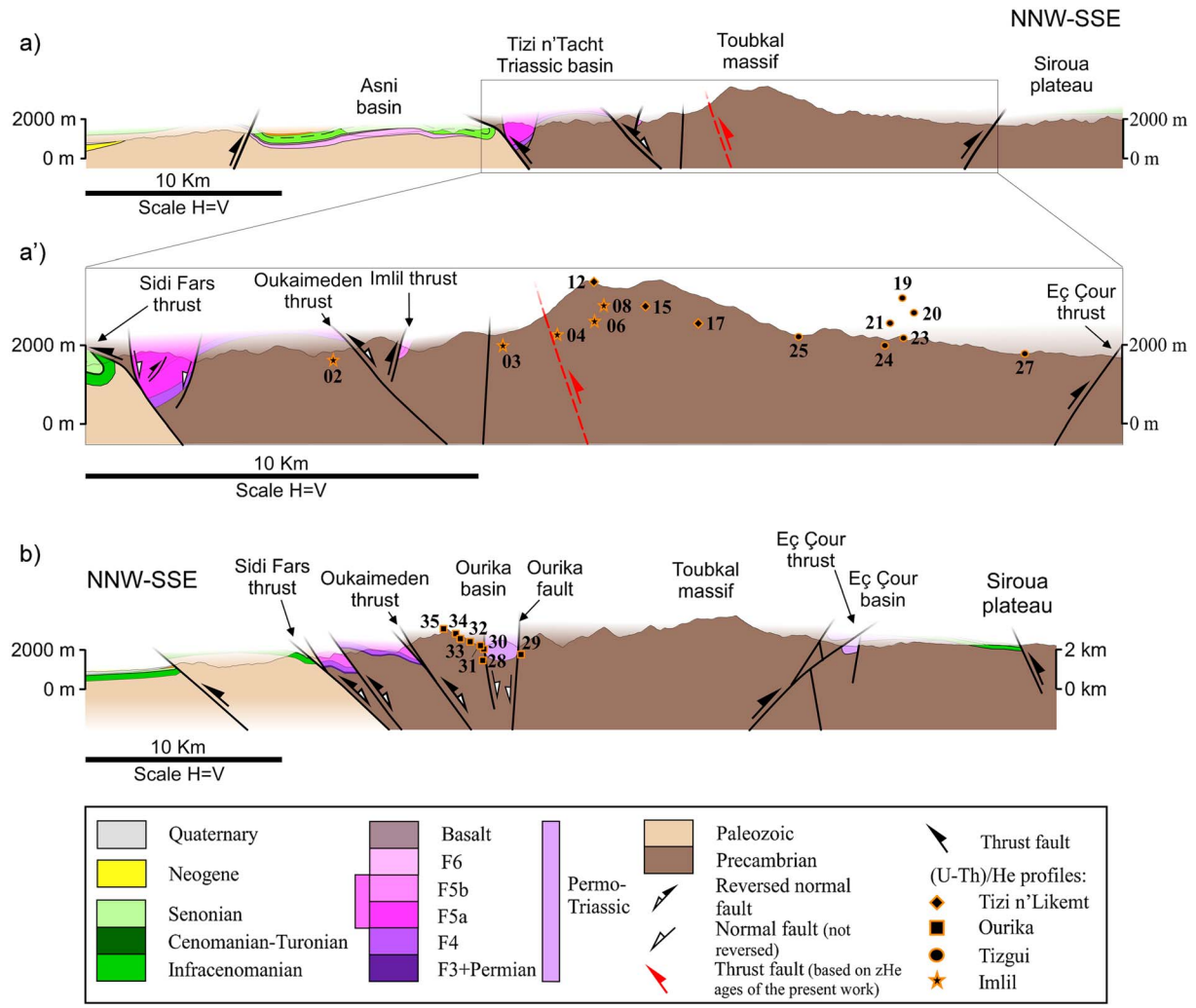

Figure 6. (a) General section of the MHA across the Tizi n'Tacht Triassic basin (which is the western continuation of the Ourika basin) and Toubkal massif (see location in Figure 5; modified from *Domènech et al*. [2015]). (a') Close-up of the axial zone with the Imlil (stars), Tizi n'Likemt (diamonds), and Tizgui (circles) samples projected. (b) General section of the MHA across the Ourika and Eç Çour Triassic basins with the Ourika samples projected (squares; see location in Figure 5). The southern part of the section is modified from *El Arabi et al*. [2003].

MiHe-02 is separated from samples MiHe-03, MiHe-04, and MiHe-08 by the Oukaimeden and Imlil thrusts (Figures 5 and 6a). An intra-Precambrian fault is additionally deduced between sample MiHe-02 and MiHe-03-MiHe-04. The zHe ages of samples MiHe-02, MiHe-03, and MiHe-04 are elevation independent with similar ages ranging from 85.7 ± 6.9 Ma to 131.8 ± 10.5 Ma (Figure 7b), suggesting that these samples resided at above the zPRZ during the Atlas orogeny and do not record any cooling associated with displacement along the Imlil and Oukaimeden thrusts in this locality. In contrast, the structurally highest sample (MiHe-08) has two aliquots with ages of 24.8 ± 2.0 and 43.7 ± 3.5 Ma, clearly exhibiting the imprint of the Atlas orogeny and recording the thermal history of a different structural block and hence cannot be jointly modeled.

The three samples of the Tizi n'Likemt elevation profile (samples MiHe-12 to MiHe-17) are from the highest reaches of the Ourika river up to the Tizi n'Likemt mountain pass, between 2559 and 3629 m of elevation (diamonds in Figures 5 and 6a). Samples are from Neoproterozoic rhyolites (MiHe-12) and granites (Assarag Suite and Ouarzazate Group). ZHe ages suitable for interpretation range from 20.2 ± 1.6 Ma to 135.3 ± 10.8 Ma (Table 2 and Figure 7c). The very limited number of samples shows no positive age-elevation trend and high-elevation samples (MiHe-12 and MiHe-15) exhibit younger ages (Paleocene-early Miocene) than the low-elevation sample (MiHe-17), which yielded Cretaceous ages. This age pattern points to the existence of intrabasement faults that were active after the closure of the zHe system likely during the Cenozoic Atlas orogeny.

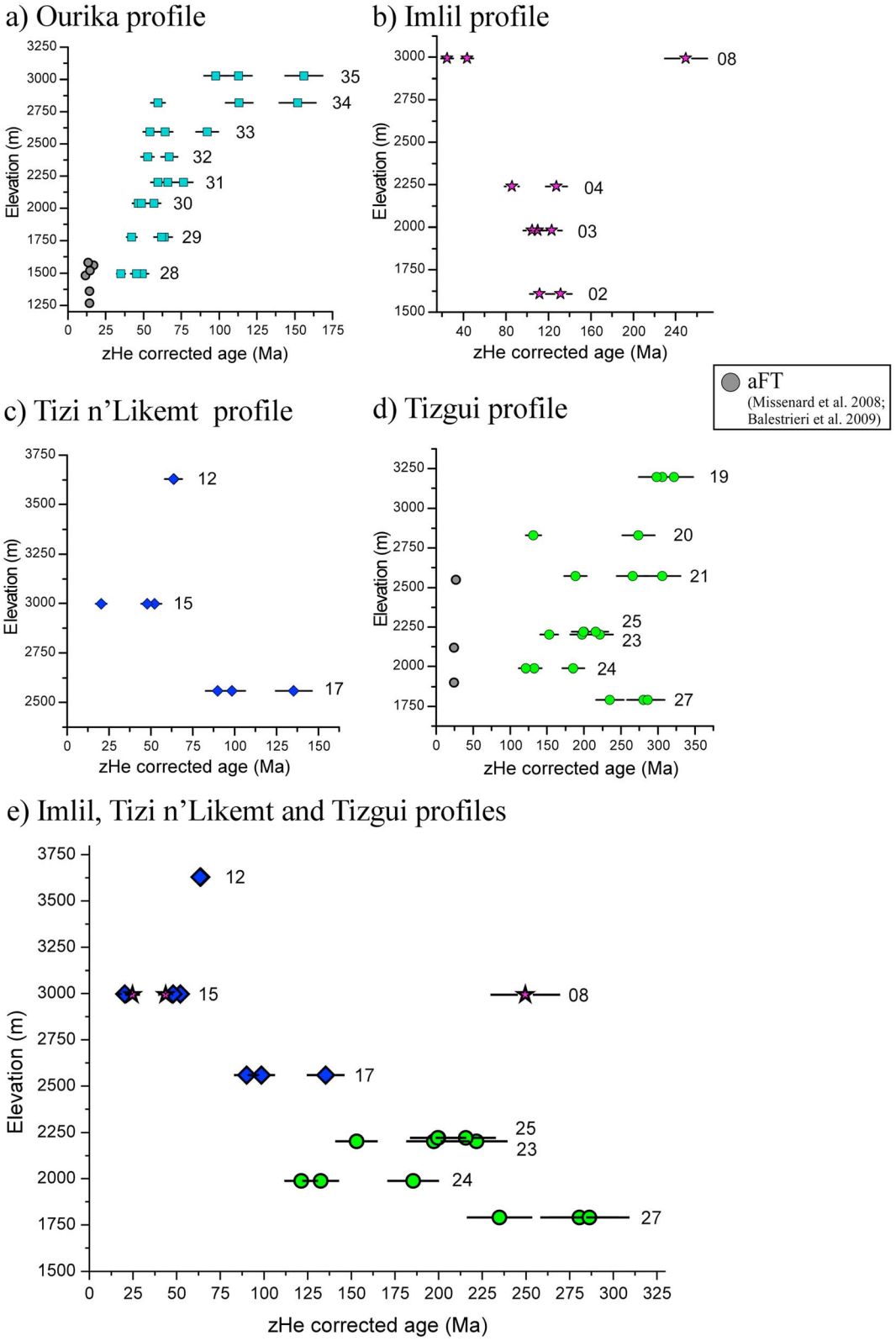

Figure 7. Age-elevation plots with 2σ error for the (a) Ourika, (b) Imlil, (c) Tizi n'Likemt, and (d) Tizgui elevation profiles. AFT data from *Missenard et al.* [2008] and *Balestrieri et al.* [2009] used in the thermal modeling are also plotted. (e) Age-elevation plots with 2σ error for the bottom samples of the Tizgui profile, the Tizi n'Likemt profile, and sample MiHe-08 of the Imlil profile showing a N-S inverse age-elevation trend (see sample location in Figure 5).

Seven samples of the Tizgui elevation profile (MiHe-19 to MiHe-27) were collected from the southern flank of the MHA in the hanging wall of the Eç Çour thrust (Figures 5 and 6a′). The Eç Çour thrust forms the southern Atlas front and was identified by *El Arabi et al*. [2003] as a south dipping normal fault which suffered a progressive inversion of its dip to the north during the Atlas compression. Due to its present gentle northward dip, we reinterpret it as a newly formed bypass thrust that cuts the former normal fault with opposite dip (Figures 6a and 6a′). Seven samples were collected from a rhyolite of the Ouarzazate Group (MiHe-19) and granites of the Assarag Suite over ~1400 m of difference in elevation along the Tizgui River (Table 2 and Figure 6a). The seven samples yielded zHe ages from 121.3 ± 9.7 Ma to 322.0 ± 25.8 Ma and intrasample grain age dispersion of 7.7% to 70.1% (Table 2 and Figure 7d). Three aFT ages previously obtained in the hanging wall of the Eç Çour thrust by *Balestrieri et al*. [2009] and *Missenard et al*. [2008] range from 24 ± 2 Ma to 26.9 ± 2.6 Ma. The zHe ages from the Tizgui elevation profile show a positive age-elevation relationship except for the bottom sample (the MiHe-27) that yielded older zHe ages (Figure 7d). Therefore, the zHe ages of the Tizgui elevation profile are considered to likely belong to same structural block and modeled as a group (except sample MiHe-27). Sample MiHe-20 is also excluded from the thermal modeling because only two zHe ages could be obtained and they present dispersion higher than 100% that cannot be accounted by differences in eU content or grain size, and which makes two aliquots not enough to be representative of the whole sample.

Combining the samples of the Tizi n'Likemt profile, the bottom samples of the Tizgui profile (samples MiHe-23 to MiHe-27), and sample MiHe-08 of the Imlil profile shows a negative age-elevation trend with zHe ages becoming progressively younger to the north and at progressively higher elevations toward the core of the High Atlas (Figure 7e).

5. Inverse Thermal Modeling

Inverse thermal modeling of the zHe ages of the Tizgui and Ourika elevation profiles was performed using the QTQt software [*Gallagher*, 2012]. In terms of the model setup, all runs were forced to end at surface temperature (20 ± 5°C) at 0 Ma. In light of the observed intrasample age overdispersion that cannot be readily explained by grain size or radiation damage variations, for modeling purposes we took into account some uncertainty in the observed zHe ages. Therefore, in order to test the robustness of the thermal models, a series of trial runs were performed using the zHe ages observed and the zHe ages resampled (see details in Text S2). As the radiation damage accumulation model for zircons of *Guenthner et al*. [2013] was only recently implemented in QTQt software and not extensively tested, thermal models were run both with and without the zircon radiation damage model. In all thermal models, the temperature difference between bottom and top samples was allowed to vary from the equivalent geothermal gradient of 10 to 40°C/km and forced to end at the surface temperatures. In some thermal models, the temperature difference between bottom and top samples was fixed over time, in others it is allowed to vary over time while maintaining a linear upper crustal geothermal gradient. The two modeled zHe elevation profiles are characterized as coherent structural blocks for which the vertical offsets between samples can be considered as invariant over time. In light of the limited horizontal distances, lateral/horizontal cooling between samples was deemed negligible. Given these assumptions, the modeled temperature difference for bottom and top samples from vertical transects can be translated into paleogeothermal gradients. Models were run for 300,000 iterations. The resulting set of thermal models with all these variables considered are included in the supporting information: Figures S1–S8. Representative models are shown in Figure 8.

5.1. Thermal Model of the Ourika Elevation Profile

A representative model of the Ourika elevation profile is presented in Figures 8a–8c. As samples were located adjacent to Triassic deposits, they were forced to be at near-surface temperatures during the latest Permian. In order to honor the aFT data available from this area [*Missenard et al*., 2008] (Figure 5), thermal histories are forced to pass through 60–120°C, which corresponds to the Apatite Fission Track Partial Annealing zone, the aPAZ [*Gleadow and Fitzgerald*, 1987], between 10 and 18 Ma.

The bottom samples (i.e., MiHe-28 to MiHe-33) are well predicted in all thermal models while the top samples (i.e., MiHe-34 and MiHe-35) are only well predicted in thermal models where the zircon radiation damage accumulation model of *Guenthner et al*. [2013] is not included (Figures 8c and S1–S4). In addition, thermal modeling including radiation damage are characterized by rapid cooling between 90 and 75 Ma from >210°C, followed by a period of slower cooling from 75 Ma to 20 Ma (Figures S1 and S2). However, cooling

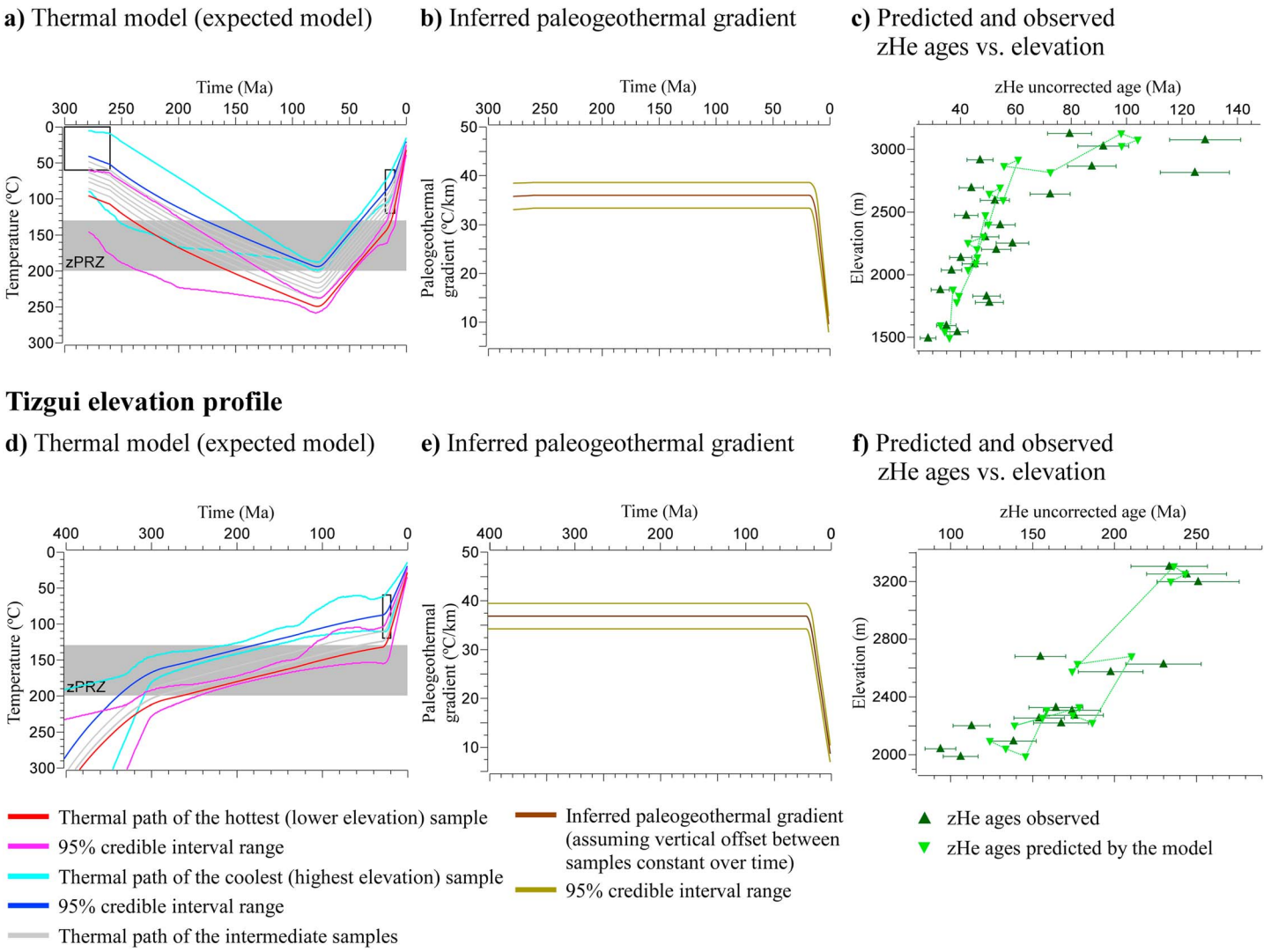

Figure 8. Inverse thermal modeling results of the (a–c) Ourika and (d–f) Tizgui elevation profiles (see location in Figure 5). The temperature between the top and bottom samples is allowed to vary between the equivalent geothermal gradient of 10–40°C/km but is fixed over time. He ages are not resampled and no radiation damage accumulation model in zircons is used (see text and Text S2 in the supporting information for explanation). Standard values of E_a and D_0 follow *Ketcham et al.* [2011]. For visualization purposes, the elevation of the aliquots with the same altitude in Figures 8c and 8f are slightly modified by the software.

from >210°C does not appear to be compatible with the high dispersion of the upper samples that suggest that they were located within the zPRZ (~130–200°C) prior to cooling. As consequence, only thermal modeling results without incorporating the radiation damage accumulation model were discussed.

The big picture extracted from these models (Figures 8a and S4) is that the thermal history is well constrained starting in the Late Cretaceous (90–100 Ma), while no reliable information can be extracted from the Ourika elevation profile for pre-Cenomanian times due to high uncertainties in the modeled *t-T* paths (which means that the zHe ages of the Ourika profile provide no information about previous thermal events). Thermal models show that basement rocks, at surface temperatures prior to the Triassic-Jurassic rifting, were subsequently reheated at some indeterminate time between Triassic to Early Cretaceous times to temperatures of 190°C to 250°C (for the top and bottom samples, respectively). After ~80 Ma (Campanian) thermal models show a continuous cooling until 20–10 Ma at mean cooling rate of 1.6–1.9°C/Ma. Due to the imposed constraint in thermal models provided by the aFT data, all model runs show an increase in cooling rate from 20 to 10 Ma

(Burdigalian-Tortonian) to present times (Figures 8a and S1–S4) at a rate of 4°C/Ma to 7°C/Ma. The deduced paleogeothermal gradient estimates are only well constrained from Late Cretaceous to Miocene times and shows high values in all thermal models performed, ranging from 30°C/km to 40°C/km (Figures 8b and S4).

5.2. Thermal Model of the Tizgui Elevation Profile

A representative model of the Tizgui elevation profile (the expected model; see Text S2 for details) is shown in Figures 8d–8f. Honoring the published aFT data [*Missenard et al*., 2008; *Balestrieri et al*., 2009], all thermal histories were forced to pass through the aPAZ between 20 and 30 Ma.

The zHe ages observed are well predicted in all thermal models (Figures 8f and S5–S8). Modeled thermal paths show that samples cooled slowly from ~300 Ma to ~120 Ma (from Permian to Early Cretaceous times) at mean rates of ~0.25–0.35°C/Ma and remained below ~130°C from Early Cretaceous to Cenozoic times. While high uncertainties exist in the modeled cooling history from the Early Cretaceous to the present, the imposed aFT constraints force the thermal model results into an increased cooling rate to 2°C/Ma–3°C/Ma from 30 to 20 Ma (Rupelian-Burdigalian) to recent times (Figures 8d and S5–S8).

The paleogeothermal gradient inferred from the different model runs shows varying evolution and high uncertainty when it is allowed to vary over time (Figures S6 and S8), which suggest that either the zHe data modeled provide insufficient precision to accurately model the gradient changes over time or that little variations in the vertical offset or horizontal cooling between samples occurred. In any case, all models indicate elevated paleogeothermal gradients of 30–40°C (Figures 8e and S6–S8).

6. Interpretation and Implications of zHe Dating and Thermal Modeling

6.1. Inferred Paleogeothermal Gradient

Thermal models for the Tizgui and Ourika elevation profiles show systematically elevated paleogeothermal gradients between 30°C/km and 40°C/km from the Triassic to Miocene. Therefore, it seems that high paleogeothermal gradients were persistent through time, not only during the rifting and associated magmatism but also during the postrift and syninversion stages. In post-Miocene times, geothermal gradient cannot be directly inferred from modeled zHe ages, but one may also expect high paleogeothermal gradients in the MHA in light of the mantle-related uplift and magmatic events that took place in the whole Atlas region since 15 Ma [*Teixell et al*., 2005; *Missenard et al*., 2006]. For that reason, and in order to enable comparison of the total amounts and rates of exhumation in different areas studied, an average geothermal gradient of 35°C/km invariant over time seems reasonable. The geological significance of the elevated paleogeothermal gradient through time is discussed below.

6.2. Tizi n'Test Area

In the Tizi n'Test area, the partial to total resetting of the zHe ages in the N'fis elevation profile (Figure 4a) indicates that samples were heated to temperatures within the zPRZ after deposition in the Triassic and prior to exhumation in the Late Jurassic. Assuming a minimum temperature of ~150–170°C for samples located at stratigraphically higher position (samples MiHe-39T and MiHe-63T located at the top of the Carnian F5b subunit), these samples had to be buried under a minimum of 3.5–4 km of rift deposits in Late Triassic to Middle Jurassic times. Therefore, taking into account the mean thickness of the F3-F5b Units in the Tizi n'Test basin of ~1–1.5 km, the total amount of Triassic-Middle Jurassic rift-related deposits which accumulated in the Tizi n'Test basin likely measured 4.5–5.5 km (Figure 9a). Assuming a total amount of 1 km of Late Triassic (post-Carnian) deposits (F6 Unit) (of which slightly over 0.5 km of thickness is preserved in the Tizi n'Test and Ourika Triassic basins [*Beauchamp*, 1988; *Benaouiss et al*., 1996; *Qarbous et al*., 2003; *Fabuel-Perez et al*., 2009; *Domènech et al*., 2015]) and basalts of the CAMP (which can be assumed to have covered the Tizi n'Test basin given their regional expansive character [e.g., *Knight et al*., 2004]), the amount of Early to Middle Jurassic deposits in the Tizi n'Test basin totaled at least 2.5–3 km (Figure 9a).

The thickness of the rift-related deposits north and south of the Tizi n'Test basin can be estimated from the combination of geological and thermochronometric constraints. The Cambrian sample of the Al Mdad profile, located south of the Tama'rout thrust preserves Variscan orogeny related Carboniferous-Permian zHe ages (Table 1) and hence was not buried to more than ~3 km (~130°C) during and after Triassic-Jurassic rifting. Published apatite and zircon FT and (U-Th)/He ages from the Anti-Atlas document cooling of samples

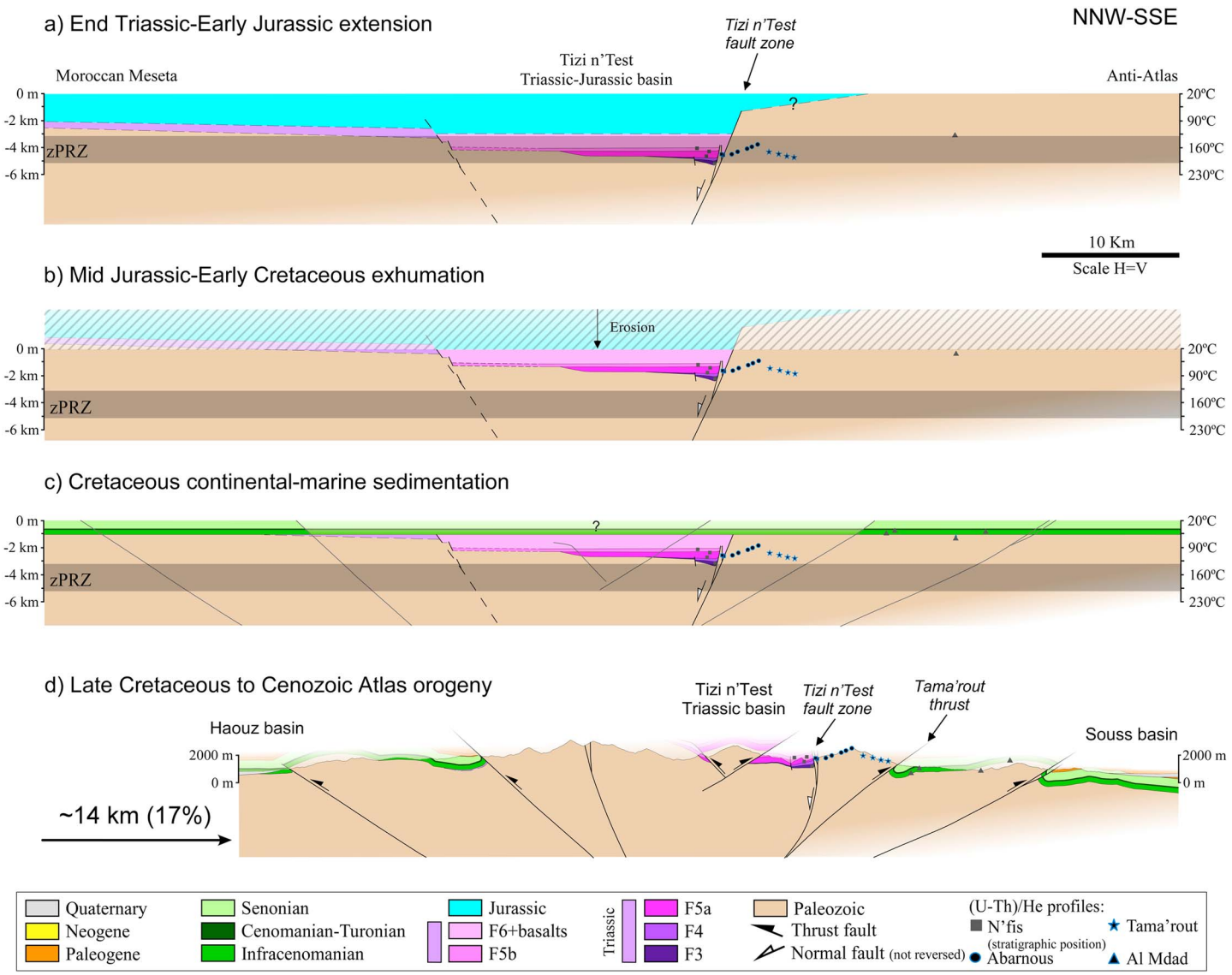

Figure 9. Cross sections of the MHA across the Tizi n'Test Triassic basin restored to selected steps based on zHe data interpretation (see location in Figure 2). The location of samples at each step according to their zHe age is also shown. (a) Restored cross section to the end of the Triassic-Mid Jurassic extension. The southern border of the Jurassic sedimentation area cannot be precisely delimited (see text for explanation). (b) After Mid-Late Jurassic to Early Cretaceous exhumation. (c) After Early to Late Cretaceous continental-marine sedimentation. We assume that some sedimentation occurred also in the axial zone of the MHA, in spite of the fact that Cretaceous deposits are rarely preserved (see text for discussion). (d) Present-day cross section.

from Carboniferous to Early Cretaceous [*Malusà et al.*, 2007; *Ghorbal*, 2009; *Sebti et al.*, 2009; *Ruiz et al.*, 2011; *Sebti*, 2011; *Oukassou et al.*, 2013; *Sehrt*, 2014; *Gouiza et al.*, 2016], suggesting that the Anti-Atlas formed the shoulder of the Atlas rift and that little to no deposition of Triassic-Jurassic rocks occurred south of Tama'rout thrust (Figure 9a). However, the data cannot ascertain whether the Triassic-Jurassic deposits extended immediately south of the Tizi n'Test fault, as the Abarnous and Tamarout zHe ages were reset in the Late Jurassic, and it is thus unclear whether the samples were buried by Triassic-Jurassic or Paleozoic rocks (or the two; see Figure 9a).

To the north, aFT and aHe ages and thermal models in basement rocks of the Moroccan Meseta and the MHA foothills revealed Middle Jurassic-Early Cretaceous cooling [*Ghorbal et al.*, 2008; *Saddiqi et al.*, 2009; *Barbero et al.*, 2011; *Bertotti and Gouiza*, 2012]. These studies showed that the Moroccan Meseta and foothill samples were locally overlain by Triassic or Early Cretaceous to Cenomano-Turonian deposits (Figure 1) and thus were near the surface in pre-Triassic and Cretaceous times. Therefore, the samples were buried to temperatures below

or in the PAZ, causing annealing of the aFT system and reset of aHe ages, during the Triassic-Early Jurassic before cooling again to near-surface temperatures in Middle Jurassic to Early Cretaceous times. This implies that 1.5–3 km, depending on paleogeothermal gradients, of sediments were accumulated and subsequently eroded in the Moroccan Meseta and MHA foothills. Therefore, it seems likely that Triassic-Jurassic sedimentation occurred both in the Tizi n'Test basin and in the Moroccan Meseta, forming a continuous rift or sag basin. This also suggests that the Meseta cannot be considered as the emerged northern shoulder of the Atlas rift but instead represents a moderately subsiding domain during the rifting stage. However, some extensional faults likely separated the Tizi n'Test basin from the areas to the north (Figure 9a) as documented by slickensided normal fault observed near a small Triassic outcrop south of Wirgane (Figure 1) [*Domènech et al*., 2015].

The zHe ages of the N'fis, Abarnous, and Tama'rout elevation profiles (Figure 4e) suggest that rift subsidence ended in the MHA in the Middle Jurassic and was followed by rapid cooling in the Late Jurassic. Assuming a minimum temperature for the uppermost samples of the N'fis, Abarnous, and Tama'rout elevation profiles of 150–170°C (near the T_c of zHe system) at the time prior to cooling, the lowest samples had to be located at temperatures of 185–200°C, considering the present vertical offset in Paleozoic samples and the pretilting offset in the Triassic samples. This implies a minimum amount of cooling of 55°C to 70°C during the Late Jurassic to bring all samples above the zPRZ, which is translated into $>$1.5–2 km. Estimating that ~1–1.5 km of Cretaceous (postexhumation) or younger sediments accumulated in the axial part of the MHA, based on the thicknesses exposed in the northern and southern foothills (Figure 3), then the amount of total exhumation increases to 2.5–3.5 km (Figures 9b and 9c).

While one might consider postrift thermal relaxation to explain Late Jurassic cooling, the amount of cooling registered by the zHe data cannot be fully explained by a decrease in the paleogeothermal gradient, requiring more significant cooling driven by "real" exhumation. In addition, the modeled paleogeothermal gradients for the Ourika elevation profile (Figures 8a–8c and S1–S4) are persistently high (30–40°C/km) in the Late Cretaceous, and thus, the amount of exhumation calculated appears to be realistic. This cooling and exhumation is regionally supported by Middle Jurassic-Early Cretaceous aHe and aFT ages in the Moroccan Meseta, the southern and northern MHA foothills, and the Anti-Atlas [*Malusà et al*., 2007; *Ghorbal et al*., 2008; *Balestrieri et al*., 2009; *Sebti et al*., 2009; *Ghorbal*, 2009; *Saddiqi et al*., 2009; *Barbero et al*., 2011; *Sebti*, 2011; *Ruiz et al*., 2011; *Bertotti and Gouiza*, 2012; *Oukassou et al*., 2013; *Sehrt*, 2014; *Gouiza et al*., 2016]. All these results define a wide region of cooling, requiring kilometer-scale upward vertical movements with exhumation during the Middle Jurassic-Early Cretaceous times that spans from the Moroccan Meseta to the Anti-Atlas, crossing the MHA (Figure 9b). In addition, the 1.5–3.5 km of exhumation calculated from the new zHe data is in agreement with the estimated exhumation values of 1.5 to ~3 km proposed for the Moroccan Meseta and the MHA foothills by *Ghorbal et al*. [2008], *Saddiqi et al*. [2009], and *Bertotti and Gouiza* [2012].

The onset of the Atlas orogeny and the amount of related exhumation in the Tizi n'Test area are poorly constrained by zHe ages as all samples have cooled to temperatures below the zPRZ by the Late Jurassic and thus cannot quantify the final exhumation related to the Atlas orogeny. However, some inferences can still be made. First, the total amount of exhumation, related to both tectonic thickening and potentially mantle-related uplift, in the Tizi n'Test basin and adjacent southern Paleozoic basement (north of the Tama'rout thrust) is $<$3 km, as all samples were at temperatures lower than ~130°C by the Early Cretaceous. Second, south of the Tama'rout thrust, the Paleozoic sample of the Al Mdad profile resided at near-surface temperature prior to Infracenomanian sedimentation and were covered by 1–1.5 km of Cretaceous to Tertiary deposits, preserved in the Sub-Atlas zone of the MHA above the sample (Figures 2 and 3). This implies a total amount of Cenozoic exhumation of ~1–1.5 km. As the Cenozoic uplift and exhumation, potentially produced by a mantle upwelling, is expected to be equal in the whole MHA, given the long-wavelength character of a mantle-related anomaly, the difference in exhumation of 1.5–2 km across the Tama'rout thrust can likely be attributed to the activity of the Tama'rout thrust and provide an estimate for the vertical displacement along this fault. Given the current fault dip (~30–35°C) observed at the surface, this implies a net slip on the thrust plane of 3–4 km. Integrating this with the reconstruction of the Atlas rift and the Middle Jurassic to Early Cretaceous exhumation, the restored cross section (Figures 9c and 9d) indicates a total shortening of ~14 km (~17%) for the High Atlas in the Tizi n'Test transect. Minimum displacement has been assigned for thrusts in the northern and southern foothills of the Atlas on the basis of post-Paleozoic sediments preserved.

6.3. Ourika-Toubkal Area

Thermal modeling of the Tizgui elevation profile (Figures 8d–8f) shows that rocks progressively cooled from Permian to Early Cretaceous times at rates of ~0.25−0.35°C/Ma (exhumation of 0.007–0.01 mm/a), which implies that during the Triassic and Jurassic rifting the area was a slowly exhuming structural high or horst block.

Samples MiHe-02 to MiHe-04 from the Imlil elevation profile (Figure 7b) exhibit mainly Early Cretaceous zHe ages that are invariant with altitude, implying that samples were at temperatures higher than ~200°C after the Triassic-Jurassic rift and prior to rapid Early Cretaceous cooling. Sample MiHe-02 from the footwall of the Oukaimeden reverse normal fault and 300 m below the F4 Triassic unit, which lies unconformable on basement in the Tizi n'Tacht basin (Figure 5), recorded near-surface temperature in Permian times prior to being heated to a >200°C during Early Mesozoic rifting. This requires that >5 km of Triassic-Jurassic rift sediments were deposited in Oukaimeden area. Assuming ~2 km of Triassic rocks, based on the thickness of the lower deposits preserved in the Ourika Triassic basin and a maximum of ~1 km for the top F6 Unit and basalts [*Beauchamp*, 1988; *Benaouiss et al*., 1996; *Fabuel-Perez et al*., 2009], this indicates that ~3 km of Jurassic sedimentary rocks accumulated in the Tizi n'Tacht basin in the footwall of the Oukaimeden fault. There is no stratigraphic datum to constrain the position of samples MiHe-03 and MiHe-04 during Triassic-Jurassic rifting prior to their Early Cretaceous cooling as none of these samples are overlain by Triassic deposits and they are separated from sample MiHe-02 by at least one intra-Paleozoic fault and Tertiary thrusts (Figures 5 and 6a). However, these samples cooled through the zPRZ (>200°C to <130°C) in the Early Cretaceous, implying a total amount of exhumation >2 km during that time interval. The magnitude of exhumation calculated from these Early Cretaceous zHe ages is similar to estimates obtained from the Tizi n'Test area and the northern and southern MHA foothills, as well as the Moroccan Meseta and the Anti-Atlas.

Combining the results of the thermal models of the Tizgui and Ourika elevation profiles and the zHe ages obtained for the Imlil profile (Figures 7 and 8) allows for a stepwise restoration of the Ourika area from Triassic-Jurassic extension to the present (Figure 10). For this restoration, sample MiHe-02 is projected into the cross section as it directly constrains the amount of Triassic-Jurassic accumulation in the footwall of the Oukaimeden normal fault. The modeling of the Ourika elevation profile, located in the hanging wall of the Oukaimeden fault, and the single-grain age dispersion of structurally shallow samples of this profile indicates that the top samples were located near the lower limit of the zPRZ, limiting their burial depth to <4.5–5 km prior to their exhumation starting at ~80 Ma (Campanian) (Figure 10c). As these samples resided at near-surface temperatures prior to the Triassic-Jurassic rifting, the implication is that they were dramatically buried in Triassic-Jurassic times before being exhumed in the Middle Jurassic-Early Cretaceous (>2 km) and probably reburied under thin Cretaceous deposits (~500 m) (as seen in the preserved record of the foothills; Figure 6). Therefore, it is necessary that these samples were buried under >6 km (for the top sample) of Triassic-Jurassic rocks in order to keep them at ~4.5–5 km deep after the Middle Jurassic to Cretaceous exhumation and burial events (Figure 10). This implies >4 km of Jurassic sediment accumulated in the Oukaimeden hanging wall (Figure 10a). Furthermore, in this reconstruction (Figure 10a) the boundary between the Ourika basin and the Toubkal horst (represented by the Tizgui thermal model; Figures 8d–8f) is well defined in the Ourika basin and represented by the Ourika fault, which has been interpreted as a normal fault during the extension based on field evidence and microstructural analysis [*Domènech et al*., 2015].

Based on the preorogenic restored cross section (Figure 10c) and the present-day cross section (Figure 10d), the total amount of shortening in this transect of the High Atlas mountains totals at least ~13 km (21%). For the southern and northern thrust faults (Figure 10d), whose hanging wall cutoffs cannot be constrained by thermochronologic ages, the restoration relies on minimum displacement estimates.

The zHe ages and modeled thermal paths from the Ourika and Tizgui elevation profiles, with aFT data of *Missenard et al*. [2008] and *Balestrieri et al*. [2009] included as constraints (Figure 8), show major differences between the northern and southern MHA flanks in terms of the magnitude and rate of exhumation related to the Atlas orogeny. The Ourika thermal model shows exhumation rates from Campanian to Burdigalian-Tortonian of 0.04–0.06 mm/a (1.6–1.9°C/Ma), implying ~3–3.5 km of total exhumation, and rates from the Burdigalian-Tortonian to the present of 0.1–0.2 mm/a (4°C–7°C/Ma), totaling 1–3 km of exhumation for bottom and top samples. Meanwhile, the Tizgui thermal model indicates that samples were at maximum depths of ~2–3 km for the top and bottom samples, respectively, in Early Cretaceous times, as the bottom sample

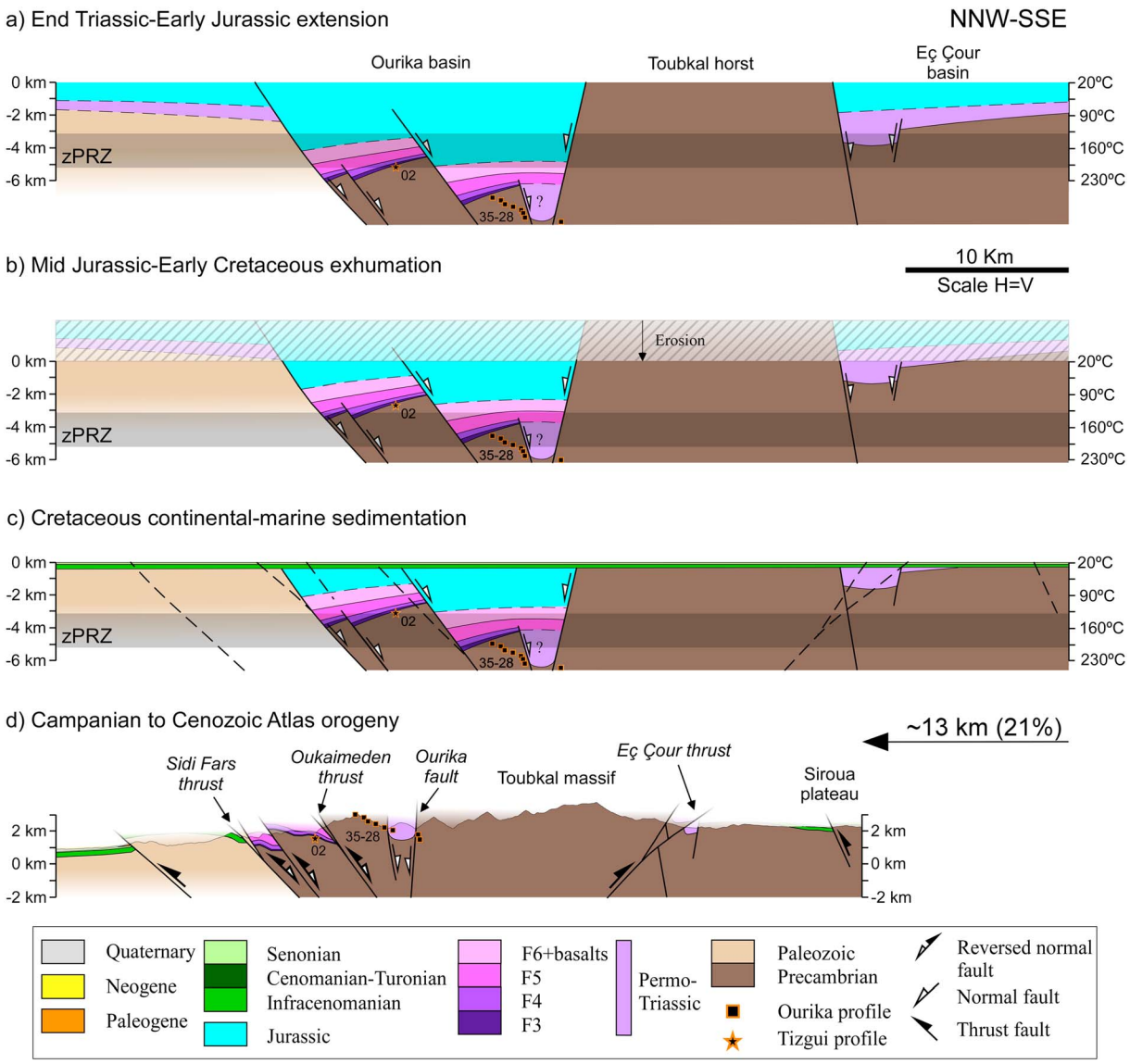

Figure 10. Postrift to present reconstructed section for the MHA across the Ourika Triassic basin and Toubkal horst in selected steps aided by thermochronology. Black squares and stars show the location of samples at every stage based on their zHe age and the Ourika thermal model (see location in Figure 5). The Toubkal horst, placed in between the Ourika and Eç Çour Triassic basins, is supported by the zHe ages and thermal models obtained for the Tizgui elevation profile (see text for explanation).

had to be located at less than ~130°C. Derived exhumation rates of 0.06–0.09 mm/a (2°–3°C/Ma) from Rupelian-Burdigalian to present times add up to exhumation amounts of ~1 km to 3 km. This implies that pre-Oligocene exhumation was limited to $<$1 km.

Furthermore, the composite north-south age-elevation profile combining the bottom samples of the Tizgui elevation profile (samples MiHe-23 to MiHe-27), the Tizi n'Likemt profile (MiHe-15 and MiHe-17), and sample MiHe-08 of the Imlil profile (Figure 7e), recording an inverted/negative age-elevation trend, documents a progressive increase in magnitude of exhumation from south to north. This trend of increasing exhumation toward the core of the High Atlas may have been caused by a south vergent thrust fault during Paleocene to early Miocene, as recorded by samples MiHe-15, MiHe-12, and MiHe-08 (Table 2 and Figure 7e). Tilting is thus related to the compressional stage and related to Tertiary active thrusting. Therefore, a main thrust is tentatively placed in Figure 6 between samples MiHe-08 and MiHe-04. This thrust was not mapped before and is also shown tentatively in the map of Figure 5. Its lateral continuation cannot be precisely traced with the available observations. The slightly older zHe ages of sample MiHe-12 compared with the other samples

of the Tizi n'Likemt profile and sample MiHe-08 (Figure 7e) could indicate the existence of a related subsidiary thrust fault between samples MiHe-12 and MiHe-15 (Figure 5). The total amount of exhumation and the degree of tilting produced by the thrust cannot be precisely determined due to the lack of paleodepth and paleotemperature constraints prior to Tertiary exhumation. However, it can be inferred that the exhumation for sample MiHe-27 was limited to <3 km, as it resided at <130°C during the compressional stage. On the other hand, the Paleocene-Early Miocene ages of samples MiHe-15, MiHe-12, and MiHe-08 indicate that they were cooled from temperatures >200°C and experienced total exhumation of >5 km during the Tertiary. Therefore, the differential exhumation of at least 2 km between northern and southern samples in the inverted age-elevation profile represents a minimum amount of exhumation produced by tilting.

7. Discussion

7.1. The Tizi n'Test Fault Zone

In the Tizi n'Test area, similar ages from the Triassic and Paleozoic samples in the N'fis, Abarnous, and Tama'rout elevation profiles (mean cooling age of 154 ± 43 Ma) from both sides of the Tizi n'Test Triassic basin-bounding normal faults (Figures 1 and 3), imply that vertical movements on these faults have been relatively minor since the Late Jurassic. Similarly, all zHe ages from both sides of the Ourika fault appear to share the same thermal history, demonstrating that the Ourika fault, which is part of the Tizi n'Test fault zone, experienced no major vertical movements since the Late Cretaceous. These results are in agreement with recent field observations and microstructural analysis by *Domènech et al*. [2015] that showed that major faults belonging to the Tizi n'Test fault zone were active as normal faults during the rifting stage but experienced no to only very limited movement during the Tertiary Atlas orogeny. Importantly, this argues against previous interpretations of the Tizi n'Test fault as a major Tertiary thrust fault [*Laville et al*., 1977; *Proust et al*., 1977; *Binot et al*., 1986; *Froitzheim et al*., 1988; *Qarbous et al*., 2008], a major transpressive fault with a modest left strike-slip movement [*Mattauer et al*., 1977], or as a dextral transpressive fault still active in the Quaternary [*Delcaillau et al*., 2011].

7.2. The Triassic-Jurassic Rift

The zHe ages and modeling results obtained in the MHA reveal that >5–6 km of Triassic-Jurassic rift-related sediments were deposited in the present-day Ourika basin (Figure 10a). To the west, in the Tizi n'Test basin, Triassic-Jurassic accumulations are similarly estimated to >4.5 km (Figure 9a). This means that assuming a maximum thickness of Triassic red beds of ~2 km [e.g., *Domènech et al*., 2015], the reconstructed thickness of Jurassic rocks ranges from 2.5 km to more than 4 km from west to east. These findings constitute the first estimation of the total rift-related sediment thickness in the MHA and show that the rift was fully developed in the area and clearly demonstrating that a marine or continental connection existed between the Atlantic (Western High Atlas) and Tethys (Central Eastern High Atlas) rifts. This conclusion is in contrast to previous reconstructions which suggested that the MHA was a structural high during the Triassic-Jurassic rifting [*Choubert and Faure-Muret*, 1962; *Du Dresnay*, 1971; *Michard*, 1976; *Stets*, 1992; *Jabour et al*., 2004; *Laville et al*., 2004; *El Arabi*, 2007; *Frizon de Lamotte et al*., 2008, 2009; *Baudon et al*., 2012].

Thermal modeling of the Tizgui elevation profile (Figures 8d–8f) shows that rocks were progressively exhumed from Carboniferous to Lower Cretaceous times at low rates (0.007–0.01 mm/a). These results confirm the previous reconstructions based on sedimentary data [*Stets*, 1992; *El Arabi et al*., 2003; *Frizon de Lamotte et al*., 2009; *Domènech et al*., 2015] that suggested a paleohigh in the present Toubkal massif area, separating the northern (the Ourika-Tizi n'Tacht) and southern (the Eç Çour) Triassic rift basins (Figure 10). The reconstructed cross sections (Figures 9 and 10) show that the main Mesozoic rift trough largely followed the transition zone between the Moroccan Meseta and Anti-Atlas domains, including the northward deflection around the Ouzellarh Precambrian salient in the MHA. This influence or control of the Variscan structural grain and anisotropy on the location/orientation and development of early Mesozoic rift was also discussed in *Domènech et al*. [2015].

7.3. The Middle Jurassic to Early Cretaceous Exhumation

A long-wavelength, kilometer-scale region of uplift with exhumation of ~1.5–3.5 km of rocks during the Middle Jurassic to Early Cretaceous is documented for the first time in the MHA inner belt by zHe ages (Figures 4e and 7b). Based on this and previous published thermochronometric data [*Malusà et al*., 2007;

Ghorbal et al., 2008; *Balestrieri et al*., 2009; *Sebti et al*., 2009; *Ghorbal*, 2009; *Saddiqi et al*., 2009; *Barbero et al*., 2011; *Sebti*, 2011; *Ruiz et al*., 2011; *Bertotti and Gouiza*, 2012; *Oukassou et al*., 2013; *Sehrt*, 2014; *Gouiza et al*., 2016], the area affected by this exhumation event spans from the Moroccan Meseta to the Anti-Atlas, crossing the MHA (Figures 9b and 10b), nearly parallel to the Atlantic margin. The Middle Jurassic-Early Cretaceous period of exhumation coincides with a deceleration in subsidence or sedimentary hiatus in the Central and Eastern High Atlas as exemplified by Bathonian to Albian red bed deposition of the so-called "couches rouges" formation [*Jenny et al*., 1981; *Haddoumi et al*., 1998, 2002, 2008, 2010; *Andreu et al*., 2003; *Charrière et al*., 2005], and with a continuous or accelerating subsidence in the Western High Atlas and deposition of marine carbonates with episodes of clastic influx [*Price*, 1981; *Davison*, 2005; *Bouatmani et al*., 2007; *Frizon de Lamotte et al*., 2009; *Bertotti and Gouiza*, 2012]. The abundance of pre-Mesozoic clasts in the couches rouges formation [e.g., *Choubert and Faure-Muret*, 1962] and in siliciclastic sediments of the Atlantic shelf [*Price*, 1981; *Davison*, 2005] supports our proposed notion of widespread erosion during this period of time. Subsequent marine to continental sedimentation of the Infracenomanian Unit (Barremian-Aptian to Early Cenomanian) [*Roch*, 1939; *Gauthier*, 1960; *Choubert and Faure-Muret*, 1962; *Ettachfini and Andreu*, 2004] in the Central High Atlas and in the western Moroccan domain above a low-relief unconformity suggests that it postdates the widespread Middle Jurassic to Early Cretaceous exhumation and that unconformity represents a regional low-relief planation surface across the exhumed area (Figures 9c and 10c).

The causes of this Middle Jurassic to Early Cretaceous exhumation are not yet fully understood. *Bertotti and Gouiza* [2012] attributed it to E-W shortening superimposed on the postrift subsidence of the Atlantic margin, based on the observation of a few synsedimentary structures (meter-scale folds and minor thrusts) in the Middle Jurassic to Lower Cretaceous formations of the Essaouira-Agadir basin (Figure 1). However, no E-W trending compressional structures belonging to this period of time are observed in the MHA and elsewhere, and the meter-scale folds and thrusts reported could alternatively have been caused by diapirism, as proposed by *Hafid et al*. [2006]. Salt-related structures have also been identified in the Central High Atlas and along the Atlantic margin [*Courel et al*., 2003; *Tari et al*., 2003; *Hafid et al*., 2006; *Tari and Jabour*, 2013; *Saura et al*., 2014]. *Frizon de Lamotte et al*. [2009] proposed a thermal origin for the regional uplift and exhumation, supported by magmatic activity in the Central High Atlas during the late Middle Jurassic to Early Cretaceous. The persistent elevated paleogeothermal gradients observed in our thermal modeling since Late Permian times suggest anomalous basal heat flow condition through time that could lend support to the thermal doming interpretation, although magmatism has not been observed within the exhuming domains as basalts are found only in the Central High Atlas. However, the lack of magmatic rocks could be explained by the fact that Jurassic-Cretaceous magmatic bodies appear to have been emplaced at shallower depths in the Jurassic sedimentary pile that has since been eroded from the MHA, leaving little evidence in the Paleozoic basement. This is similar to rift-related late Triassic magmatism. In the Central High Atlas, evidence for Middle Jurassic-Early Cretaceous uplift appears to be masked by synrift to postrift thermal subsidence, as net subsidence and sedimentation, although with some hiatuses, persisted at lower rates.

Alternatively, the differential subsidence between the Western and Central High Atlas and the intervening uplifted erosional belt, parallel to the Atlantic margin, may be intrinsically related with the Atlantic rift. Rifting in the Atlantic margin is reported to end in the Early Jurassic [*Stets*, 1992; *Medina*, 1995; *Piqué and Laville*, 1996; *Le Roy and Piqué*, 2001; *Tari et al*., 2003; *Hafid et al*., 2006; *El Arabi*, 2007; *Tari and Jabour*, 2013] in response to the onset of seafloor spreading and formation of Atlantic oceanic crust between 195 Ma and 170 Ma [*Medina*, 1995; *Sahabi et al*., 2004; *Davison*, 2005]. However, there are numerous cases along the rift flanks of the Atlantic and other oceans where uplift, peneplanation, and burial occurred during postrift times [e.g., *Green et al*., 2013, and references therein]. While the causes of these vertical movements are not fully understood, *Green et al*. [2013] suggested as possible causes (1) lithosphere-scale folding either propagating from orogenies elsewhere or from basal drag of the lithosphere by horizontal asthenospheric flow, (2) flexural isostatic response to local erosion onshore (e.g., from rift flank escarpment retreat) and sediment loading offshore, and (3) thermal doming associated to a mantle plume and/or hot underlying asthenosphere. We suggest that the Middle Jurassic-Early Cretaceous exhumation belt in Morocco could be effectively due to large-scale mantle doming combined with flexural isostatic response to sedimentary loading along the Atlantic margin offshore.

7.4. The Atlas Orogeny

The onset of the Atlas compression-driven exhumation is constrained in the Ourika thermal model as the Campanian (Figures 8a–8c). This appears to coincide with deposition of Senonian red beds in the Atlas domain and is consistent with widespread compressional tectonics in Africa during this time [e.g., *Guiraud and Bosworth*, 1997]. Local exposure of Senonian growth strata and an unconformity at the base of the overlying Eocene carbonates has been reported in the High and Middle Atlas [*Laville et al*., 1977; *Froitzheim et al*., 1988; *Herbig*, 1988]. However, these features are only locally observed and no major foreland basins developed at this time. This is not incompatible with the results presented here. Slow exhumation rates (0.04–0.06 mm/a) obtained for the Ourika thermal model from Late Cretaceous to Miocene suggests the possible coexistence of localized exhumation in the inner parts of the Atlas belt, with a few emergent structures, and sedimentation on a broad continental-marine shelf without the development of a major flexural foredeep. Similar late Turonian to early Eocene aFT ages from the Central High Atlas axial zone [*Barbero et al*., 2007] were suggested to record postrift/postmagmatic cooling, as they define continuous cooling since the Late Jurassic, but in fact they could also be attributed at least in part to Late Cretaceous early Atlas orogeny.

The restored cross sections presented in Figures 9 and 10 show values of orogenic shortening of ~13 km to ~14 km (~21% to ~17%), which are consistent with values reported for the Central High Atlas of 30 to 13 km (24 to 15%) [*Teixell et al*., 2003]. The thermochronology-based deduction of basement thrust faults that were not observed previously in field surveys (Figure 7e) suggests that these shortening estimates are minimum values, although the high-angle style of reverse faulting observed and the similar structural level exposed suggest that it is unlikely that major large-displacement structures have been overlooked.

The total amount of exhumation estimated along the northern and southern flanks of the MHA across the Ourika Triassic basin and Toubkal massif (Figure 10) have major implications for the Atlas orogenic development. The data indicate that while the northern thrust faults started moving in the Late Cretaceous to Paleocene (Figures 7 and 8), the southern Eç Çour thrust was not active until the Oligocene, suggesting that early shortening and associated exhumation was mainly focused along the northern flank. The aFT data included in thermal models show that exhumation accelerated from the Oligocene-Miocene to the present along the northern and southern flanks, with similar total amounts of exhumation, attesting to coeval bivergent movement of the northern and southern thrust systems. These results are consistent with structural geology and recent magnetostratigraphy of the tectonosedimentary record in foreland basin deposits associated with the external thrust belt in the northern Ouarzazate basin [*Tesón and Teixell*, 2008; *Tesón et al*., 2010]. However, the total amount of exhumation from Oligocene to recent times cannot be completely attributed to thrust-related exhumation as part of it may be related to dynamic mantle-driven uplift since 15 Ma [*Teixell et al*., 2005; *Missenard et al*., 2006].

The dominant north directed vergence of the main thrusts in the Ourika-Toubkal area is in agreement with the higher magnitude of exhumation along the northern flank. This compressional geometry was influenced by the inherited Variscan structural grain and the Triassic rift configuration (i.e., the horst-graben geometry observed). The Ouzellarh Precambrian salient could have acted as a backstop to the south of the High Atlas belt, promoting the northward propagation of the deformation. The fact that the highest summits of the High Atlas are located in the Toubkal massif and are located outside of the modeled maximum mantle-driven uplift zone [*Missenard et al*., 2006; *Fullea et al*., 2007] can be explained as reflecting the inherited rifting structure and the focusing of the compressional crustal thickening in a narrow area around the Ouzellarh massif along the border of the Variscan domain.

8. Conclusions

Zircon (U-Th)/He data have been obtained from 42 samples of basement and Triassic rocks of the Marrakech High Atlas from eight profiles following two regional NNW-SSE transects across the Atlas mountain belt, separated ~45 km from each other. The zHe ages and thermal paths obtained from the modeling of elevation profiles show that the Triassic-Jurassic rift was well developed in the MHA, with accumulations of more than 4.5 to 6 km of Triassic-Jurassic deposits. This constitutes the first reliable estimation of the total amount of rift sedimentary thickness in the MHA and demonstrates that the Tethys (Central Eastern High Atlas) and

Atlantic (Western High Atlas) rifts were connected in Triassic to Middle Jurassic times. The horst-graben geometry in the present Toubkal massif and Ourika-Tizi n'Tacht Triassic basins is also evidenced by thermochronology. Based on the Triassic-Jurassic Tizi n'Test and Ourika basin reconstruction assisted by thermochronology, we deduce a major influence of inherited Variscan structural grain and rheologic anisotropy, including the Ouzellarh Precambrian salient, on rift development and orientation, which, in turn, influenced the subsequent contractional Atlas orogenic configuration.

Consistent Late Jurassic to Early Cretaceous zHe cooling ages obtained in the Tizi n'Test and Ourika-Toubkal areas indicate that the rift-related subsidence in the MHA ended by Middle Jurassic times and was followed by a period of kilometer-scale exhumation (1.5–3.5 km). These zHe ages are in agreement with published aFT and aHe ages from the Moroccan Meseta, the Anti-Atlas, and also the foothills of the MHA, and together define a Middle Jurassic to Early Cretaceous exhuming paleohigh in these areas that is roughly parallel to the Atlantic margin.

ZHe ages and thermal modeling reveal a localized, moderate exhumation event starting in the Campanian and provide the first thermochronometric clue for a Late Cretaceous initiation of the Atlas contractional deformation and exhumation in the inner parts of the High Atlas. Exhumation continued during the Paleocene-Eocene and is accelerated since the Oligocene or Miocene, consistent with dated tectonic-sedimentation relationships in the external thrust belts of the High Atlas. Thermochronometry-assisted reconstruction of structural sections constrains the minimum values of total orogenic shortening in the MHA as 13 to 14 km (21% to 17%). ZHe ages obtained both sides of the Tizi n'Test fault zone clearly show that vertical movements and reactivation in this fault zone during the Atlas orogenic inversion stage were only very minor.

Acknowledgments

Data used in this work are listed in the references, tables, figures, and in the supporting information. This work was supported by MEC and MINECO projects CGL2014-54180-P, CGL2010-15416, CGL2007-66431-CO2-01 (TOPOMED), and Consolider-Ingenio 2010 CSD2006-00041 (TOPOIBERIA). Research by M. Domènech was funded by a predoctoral FPU grant from Ministerio de Educaci'n (Spain). We would like to thank Julien Babault for his sampling campaign and for helpful advice in early stages of this work. Alvar Pastor and Andreu Badia are thanked for field assistance. Special thanks are expressed to Kerry Gallagher for guiding into the use of the QTQt software. Marc Jolivet is gratefully acknowledged for his constructive comments and discussion of a first version of this manuscript, and the comments by Maria Laura Balestrieri and an anonymous reviewer helped to improve the original manuscript.

References

Amrhar, M. (2002), Paléocontraintes et déformations syn- et post-collision Afrique-Europe identifiées dans la couverture mésozoïque et cénozoïque du Haut Atlas occidental (Maroc), *C. R. Geosci.*, *334*, 279–285.

Andreu, B., J. P. Colin, H. Haddoumi, and A. Charrière (2003), Les Ostracodes des "Couches rouges" du synclinal d'Aït Attab, Haut Atlas Central, Maroc: Systématique, biostratigraphie, paléoécologie, paléobiogéographie, *Rev. Micropaleontol.*, *46*(4), 193–216.

Angoud, M., et al. (2002), *Carte Géologique du Maroc, Scale 1:50.000, Sheet NH-29-XXIII-1c: Tafingoult*, *Notes et Mém. 444*, Ed. du Serv. Géol. du Maroc, Rabat.

Arboleya, M. L., A. Teixell, M. Charroud, and M. Julivert (2004), A structural transect through the High and Middle Atlas of Morocco, *J. Afr. Earth Sci.*, *39*, 319–327.

Ayarza, P., F. Alvarez-Lobato, A. Teixell, M. L. Arboleya, E. Tesón, M. Julivert, and M. Charroud (2005), Crustal structure under the central High Atlas Mountains (Morocco) from geological and gravity data, *Tectonophysics*, *400*, 67–84.

Babault, J., A. Teixell, M. L. Arboleya, and M. Charroud (2008), A Late Cenozoic age for long-wavelength surface uplift of the Atlas Mountains of Morocco, *Terra Nova*, *20*, 102–107.

Balestrieri, M. L., G. Moratti, G. Bigazzi, and A. Algouti (2009), Neogene exhumation of the Marrakech High Atlas (Morocco) recorded by apatite fission-track analysis, *Terra Nova*, *21*, 75–82, doi:10.1111/j.1365-3121.2008.00857.x.

Barbero, L., A. Teixell, M. L. Arboleya, P. del Río, P. W. Reiners, and B. Bougadir (2007), Jurassic-to-present thermal history of the central High Atlas (Morocco) assessed by low-temperature thermochronology, *Terra Nova*, *19*(1), 58–64, doi:10.1111/j.1365-3121.2006.00715.x.

Barbero, L., A. Jabaloy, D. Gómez-Ortiz, J. V. Pérez-Peña, M. J. Rodríguez-Peces, R. Tejero, J. Estupiñán, A. Azdimousa, M. Vázquez, and L. Asebriy (2011), Evidence for surface uplift of the Atlas Mountains and the surrounding peripheral plateaux: Combining apatite fission-track results and geomorphic indicators in the Western Moroccan Meseta (coastal Variscan Paleozoic basement), *Tectonophysics*, *502*(1–2), 90–104, doi:10.1016/j.tecto.2010.01.005.

Baudon, C., J. Redfern, and J. Van Den Driessche (2012), Permo-Triassic structural evolution of the Argana Valley, impact of the Atlantic rifting in the High Atlas, Morocco, *J. Afr. Earth Sci.*, *65*, 91–104, doi:10.1016/j.jafrearsci.2012.02.002.

Beauchamp, J. (1988), Triassic sedimentation and rifting in the High Atlas (Morocco), in *Triassic-Jurassic Rifting*, *Dev. in Geotectonics*, vol. 22, edited by W. Manspeizer, pp. 477–497, Elsevier, New York.

Beauchamp, W., R. Allmendinger, and M. Barazangi (1999), Inversion tectonics and the evolution of the High Atlas Mountains, Morocco, based on a geological-geophysical transect, *Tectonics*, *18*, 163–184, doi:10.1029/1998TC900015.

Benaouiss, N., L. Courel, and J. Beauchamp (1996), Rift-controlled fluvial/tidal transitional series in the Oukaïmeden Sandstones, High Atlas of Marrakesh (Morocco), *Sediment. Geol.*, *107*, 21–36.

Bertotti, G., and M. Gouiza (2012), Post-rift vertical movements and horizontal deformations in the eastern margin of the Central Atlantic: Middle Jurassic to Early Cretaceous evolution of Morocco, *Int. J. Earth Sci.*, *101*(8), 2151–2165, doi:10.1007/s00531-012-0773-4.

Bertrand, H., and J. M. Prioton (1975), Les dolérites marocaines et l'ouverture de l'Atlantique: Étude pétrologique et géochimique, PhD thesis, 321 pp., Univ. Claude Bernard, Lyon, France.

Binot, F., G. Dresen, J. Stets, and P. Wurster (1986), Die Tizi-n' Test-Verwerfungszone im Hohen Atlas (Marokko), *Geol. Rundsch.*, *75*(3), 647–664.

Biron, P., and B. Courtinat (1982), Contribution palynologique a la connaissance du Trias du Haut-Atlas de Marrakech, Maroc, *Geobios*, *15*(2), 231–235.

Bouatmani, R., A. Chakor Alami, and F. Medina (2007), Subsidence, évolution thermique et maturation des hydrocarbures dans le bassin d'Essaouira (Maroc): Apport de la modélisation, *Bull. Inst. Sci. Rabat Sect. Sci. Terre*, *29*, 15–36.

Brown, R. W., R. Beucher, S. Roper, C. Persano, F. Stuart, and P. Fitzgerald (2013), Natural age dispersion arising from the analysis of broken crystals. Part I: Theoretical basis and implications for the apatite (U-Th)/He thermochronometer, *Geochim. Cosmochim. Acta*, *122*, 478–497, doi:10.1016/j.gca.2013.05.041.

Charrière, A., H. Haddoumi, and P.-O. Mojon (2005), Découverte de Jurassique supérieur et d'un niveau marin du Barrémien dans les "couches rouges" continentales du Haut Atlas central Marocain: Implications paléogéographiques et structurales, *C. R. Palevol*, *4*(5), 385–394.
Cherniak, D. J., E. B. Watson, and J. B. Thomas (2009), Diffusion of helium in zircon and apatite, *Chem. Geol.*, *268*, 155–166, doi:10.1016/j.chemgeo.2009.08.011.
Choubert, G. (1952), Aperçu structural. In: Géologie du Maroc. Notes et Mem. serv. géol. Maroc, Rabat, 100 p. et 19e Congr. géol. Intern. Alger, 3e ser., Maroc, 6, 9-73.
Choubert, G., and A. Faure-Muret (1962), Évolution du Domaine Atlasique Marocain depuis les temps paléozoïques, in *Livre à la Mémoire du Professeur Paul Fallot*, Memoire hors série, Soc. géol. France 1, Paris, 447–527.
Courel, L., H. Aït Salem, N. Benaouiss, M. Et-Touhami, B. Fekirine, M. Oujidi, M. Soussi, and A. Tourani (2003), Mid-Triassic to Early Liassic clastic/evaporitic deposits over the Maghreb Platform, *Palaeogeogr. Palaeoclimatol. Palaeoecol.*, *196*(1–2), 157–176, doi:10.1016/S0031-0182(03)00317-1.
Cousminer, H. L., and W. Manspeizer (1976), Triassic pollen date Moroccan High Atlas and the incipient rifting of the Pangea as middle Carnian, *Science*, *191*, 943–945.
Davison, I. (2005), Central Atlantic margin basins of North West Africa: Geology and hydrocarbon potential (Morocco to Guinea), *J. Afr. Earth Sci.*, *43*(1–3), 254–274, doi:10.1016/j.jafrearsci.2005.07.018.
Delcaillau, B., M. Amrhar, M. Namous, E. Laville, K. Pedoja, and O. Dugué (2011), Transpressional tectonics in the Marrakech High Atlas: Insight by the geomorphic evolution of drainage basins, *Geomorphology*, *134*(3–4), 344–362, doi:10.1016/j.geomorph.2011.07.010.
Domènech, M., A. Teixell, J. Babault, and M. L. Arboleya (2015), The inverted Triassic rift of the Marrakech High Atlas: A reappraisal of basin geometries and faulting histories, *Tectonophysics*, *663*, 177–191, doi:10.1016/j.tecto.2015.03.017.
Du Dresnay, R. (1971), Extension et développement des phénomènes récifaux Jurassiques dans le domaine Atlasique Marocain, particulièrement au Lias moyen, *Bull. Soc. Geol. Fr.*, *13*, 46–56.
El Arabi, E. H. (2007), La série permienne et triasique du rift haut-atlasique: Nouvelles datations: Évolution tectonosédimentaire, 225 pp., Univ. Hassan II Casablanca, Morocco.
El Arabi, E. H., J. Ferrandini, and R. Essamoud (2003), Triassic stratigraphy and structural evolution of a rift basin: The Eç Çour basin, High atlas of Marrakech, Morocco, *J. Afr. Earth Sci.*, *36*(1–2), 29–39, doi:10.1016/S0899-5362(03)00020-4.
El Arabi, E. H., J. B. Diez, J. Broutin, and R. Essamoud (2006), Première caractérisation palynologique du Trias moyen dans le Haut Atlas; implications pour l'initiation du rifting téthysien au Maroc, *C. R. Geosci.*, *338*(9), 641–649, doi:10.1016/j.crte.2006.04.001.
Ettachfini, E. M., and B. Andreu (2004), The Cenomanian and Turonian of the Precambrian Platform, *Cretaceous Res.*, *25*(2), 277–302.
Fabuel-Perez, I., J. Redfern, and D. Hodgetts (2009), Sedimentology of an intra-montane rift-controlled fluvial dominated succession: The Upper Triassic Oukaimeden Sandstone Formation, Central High Atlas, Morocco, *Sediment. Geol.*, *218*(1–4), 103–140, doi:10.1016/j.sedgeo.2009.04.006.
Farley, K. A. (2000), Helium diffusion from apatite: General behavior as illustrated by Durango fluorapatite, *J. Geophys. Res.*, *105*, 2903–2914, doi:10.1029/1999JB900348.
Farley, K. A., R. A. Wolf, and L. T. Silver (1996), The effects of long alpha-stopping distances on (U-Th)/He ages, *Geochim. Cosmochim. Acta*, *60*(21), 4223–4229.
Fraissinet, C., E. M. Zouine, J. L. Morel, A. Poisson, J. Andrieux, and A. Faure-Muret (1988), Structural evolution of the southern and northern Central High Atlas in Paleogene and Mio-Pliocene times, in *The Atlas System of Morocco*, edited by V. Jacobshagen, pp. 273–291, Springer, Berlin.
Frizon de Lamotte, D., B. Saint Bezar, and R. Bracène (2000), The two main steps of the Atlas building and geodynamics of the western Mediterranean, *Tectonics*, *19*, 740–761, doi:10.1029/2000TC900003.
Frizon de Lamotte, D., M. Zizi, Y. Missenard, M. Hafid, M. El Azzouzi, R. C. Maury, A. Charrière, M. Taki, M. Benami, and A. Michard (2008), The Atlas System, in *Continental Evolution: The Geology of Morocco*, *Notes in Earth Sci.*, edited by A. Michard et al., pp. 133–202, Springer, Berlin.
Frizon de Lamotte, D., P. Leturmy, Y. Missenard, S. Khomsi, G. Ruiz, O. Saddiqi, F. Guillocheau, and A. Michard (2009), Mesozoic and Cenozoic vertical movements in the Atlas system (Algeria, Morocco, Tunisia): An overview, *Tectonophysics*, *475*(1), 9–28, doi:10.1016/j.tecto.2008.10.024.
Froitzheim, N., J. Stets, and P. Wurster (1988), Aspects of Western High Atlas tectonics, in *The Atlas System of Morocco*, vol. 15, edited by V. H. Jacobshagen, pp. 219–244, Springer, Berlin.
Fullea, J., M. Fernandez, H. Zeyen, and J. Verges (2007), A rapid method to map the crustal and lithospheric thickness using elevation, geoid anomaly and thermal analysis: Application to the Gibraltar Arc system, Atlas Mountains and adjacent zones, *Tectonophysics*, *430*(1–4), 97–117.
Gallagher, K. (2012), Transdimensional inverse thermal history modeling for quantitative thermochronology, *J. Geophys. Res.*, *117*, B02408, doi:10.1029/2011JB008825.
Gallagher, K., K. Charvin, S. Nielsen, M. Sambridge, and J. Stephenson (2009), Markov chain Monte Carlo (MCMC) sampling methods to determine optimal models, model resolution and model choice for Earth Science problems, *Mar. Pet. Geol.*, *26*(4), 525–535, doi:10.1016/j.marpetgeo.2009.01.003.
Gauthier, H. (1960), Contribution a l'etude geologique des formations post-liasiques des bassins du Dades et du haut Todra (Maroc meridional), *Notes Mem. Serv. Geol. (Rabat)*, *119*, 1–137.
Ghorbal, B. (2009), *Mesozoic to Quaternary Thermo-tectonic Evolution of Morocco (NW Africa)*, 226 pp., Vrije Univ. Amsterdam, Amsterdam.
Ghorbal, B., G. Bertotti, J. Foeken, and P. Andriessen (2008), Unexpected Jurassic to Neogene vertical movements in "stable" parts of NW Africa revealed by low temperature geochronology, *Terra Nova*, *20*(5), 355–363, doi:10.1111/j.1365-3121.2008.00828.x.
Gleadow, A. J. W., and P. G. Fitzgerald (1987), Uplift history and structure of the Transantarctic Mountains: New evidence from fission track dating of basement apatites in the Dry Valleys area, southern Victoria Land, *Earth Planet. Sci. Lett.*, *82*(1–2), 1–14.
Gomez, F., W. Beauchamp, and M. Barazangi (2000), Role of the Atlas Mountains (northwest Africa) within the African-Eurasian plate-boundary zone, *Geology*, *28*(9), 775–778.
Görler, K., F.-F. Helmdach, P. Gaemers, K. Heissig, W. Hinsch, K. Mädler, W. Schwarzhans, and M. Zucht (1988), The uplift of the central High Atlas as deduced from Neogene continental sediments of the Ouarzazate province, Morocco, in *The Atlas System of Morocco*, edited by V. Jacobshagen, pp. 361–404, Springer, Berlin.
Gouiza, M., R. Charton, G. Bertotti, P. Andriessen, and J. E. A. Storms (2016), Post-Variscan evolution of the Anti-Atlas belt of Morocco constrained from low-temperature geochronology, *Int. J. Earth Sci.*, doi:10.1007/s00531-016-1325-0.
Green, P. F., K. Lidmar-Bergström, P. Japsen, J. M. Bonow, and J. A. Chalmers (2013), Stratigraphic landscape analysis, thermochronology and the episodic development of elevated, passive continental margins, *Geol. Surv. Den. Greenl. Bull.*, *30*, 1–150.
Guenthner, W. R., P. W. Reiners, R. A. Ketcham, L. Nasdala, and G. Giester (2013), Helium diffusion in natural zircon: Radiation damage, anisotropy, and the interpretation of zircon (U-Th)/He thermochronology, *Am. J. Sci.*, *313*(3), 145–198, doi:10.2475/03.2013.01.

Guiraud, R., and W. Bosworth (1997), Senonian basin inversion and rejuvenation of rifting in Africa and Arabia: Synthesis and implications to plate-scale tectonics, *Tectonophysics*, *282*(1–4), 39–82, doi:10.1016/S0040-1951(97)00212-6.
Haddoumi, H., Y. Aiméras, A.-M. Bodergat, A. Charrière, C. Mangold, and K. Benshili (1998), Ages et environnements des couches rouges d'Anoual (Jurassique moyen et Cretace inferieur, Haut-Atlas oriental, Maroc), *C. R. Acad. Sci., Ser. II. Sci. Terre Planetes*, *327*(2), 127–133.
Haddoumi, H., A. Charriere, M. Feist, and B. Andreu (2002), Nouvelles datations (Hauterivien superieur-Barremien inferieur) dans les "Couches rouges" continentales du Haut Atlas central marocain: Consequences sur l'age du magmatisme et des structurations mesozoiques de la chaine Atlasique, *C. R. Palevol*, *1*(5), 259–266.
Haddoumi, H., A. Charrière, B. Andreu, and P.-O. Mojon (2008), Les dépôts continentaux du Jurassique moyen au Crétacé inférieur dans le Haut Atlas oriental (Maroc): Paléoenvironments successifs et signification paléogéographique, Carnets de Géol./Noteb. Geol., Article 2008/06 (CG2008_A06), Brest, France.
Haddoumi, H., A. Charrière, and P.-O. Mojon (2010), Stratigraphie et sédimentologie des "Couches rouges" continentales du Jurassique-Crétacé du Haut Atlas central (Maroc): Implications paléogéographiques et géodynamiques, *Geobios*, *43*, 433–451.
Hafid, M., M. Zizi, A. W. Bally, and A. Ait Salem (2006), Structural styles of the western onshore and offshore termination of the High Atlas, Morocco, *C. R. Geosci.*, *338*, 50–64.
Harfi, A., J. L. El, and J. Salomon (1996), Le remplissage continental cenozoique du bassin d'avant-pays de Ouarzazate. Implications sur l'evolution geodynamique du Haut-Atlas Central (Maroc), *C. R. Acad. Sci., Ser. II: Sci. Terre Planetes*, *323*(7), 623–630.
Herbig, H. G. (1988), Synsedimentary tectonics in the Northern Middle Atlas (Morocco) during the Late Cretaceous and Tertiary, in *The Atlas System of Morocco*, edited by V. Jacobshagen, pp. 321–337, Springer, Berlin.
Herbig, H. G., and J. Trappe (1994), Stratigraphy of the Sub-atlas Group (Maastrichtian-Middle Eocene, Morocco), *Newsl. Stratigr.*, *30*, 125–165.
Hoepffner, C., A. Soulaimani, and A. Piqué (2005), The Moroccan Hercynides, *J. Afr. Earth Sci.*, *43*, 144–165.
Hollard, H. (1985), *Carte Géologique du Maroc-Echelle: 1/1.000.000*, Ed. Serv. Géol. du Maroc, Rabat.
Jabour, H., M. Dakki, M. Nahim, F. Charrat, M. El Alji, M. Hssain, F. Oumalch, and R. El Abibi (2004), The Jurassic depositional system of Morocco, geology and play concepts, *MAPG Mem.*, *1*, 5–39.
Jacobshagen, V., R. Brede, M. Hauptmann, and W. Heinitz (1988), Structure and post-Palaeozoic evolution of the central High Atlas, in *The Atlas System of Morocco*, edited by V. Jacobshagen, pp. 245–271, Springer, Berlin.
Jasra, A., D. A. Stephens, K. Gallagher, and C. C. Holmes (2006), Bayesian mixture modelling in geochronology via Markov chain Monte Carlo, *Math. Geol.*, *38*(3), 269–300, doi:10.1007/s11004-005-9019-3.
Jenny, J. (1983), Les décrochements de l'Atlas de Demnat (Haut Atlas central, Maroc): Prolongation orientale de la zone décrochement du Tizi n'Test et clef de la compréhension de la tectonique atlasique, *Eclogae Geol. Helv.*, *76*, 243–251.
Jenny, J., A. Le Marrec, and M. Monbaron (1981), Les couches rouges du Jurassique moyen du Haut Atlas central (Maroc): Correlations lithostratigraphiques, elements de datations et cadre tectono-sedimentaire, *Bull. Soc. Geol. Fr.*, *23*(6), 627–640.
Ketcham, R. A., C. Gautheron, and L. Tassan-Got (2011), Accounting for long alpha-particle stopping distances in (U–Th–Sm)/He geochronology: Refinement of the baseline case, *Geochim. Cosmochim. Acta*, *75*(24), 7779–7791, doi:10.1016/j.gca.2011.10.011.
Ketcham, R. A., W. R. Guenthner, and P. W. Reiners (2013), Geometric analysis of radiation damage connectivity in zircon, and its implications for helium diffusion, *Am. Mineral.*, *98*, 350–360, doi:10.2138/am.2013.4249.
Knight, K. B., S. Nomade, P. R. Renne, A. Marzoli, H. Bertrand, and N. Youbi (2004), The Central Atlantic magmatic province at the Triassic-Jurassic boundary: Paleomagnetic and Ar-Ar evidence from Morocco for brief, episodic volcanism, *Earth Planet. Sci. Lett.*, *228*, 143–160.
Laville, E., and A. Piqué (1991), La distension crustale atlantique et atlasique au Maroc au debut du Mesozoique: Le rejeu des structures hercyniennes, *Bull. Soc. Geol. Fr.*, *162*, 1161–1171.
Laville, E., J.-L. Lesage, and M. Seguret (1977), Géométrie, cinématique (dynamique) de la tectonique atlasique sur le versant sud du Haut Atlas marocain. Aperçu sur les tectoniques hercyniennes et tardi-hercyniennes, *Bull. Soc. Geol. Fr.*, *7*(t.XIX), 527–539.
Laville, E., A. Piqué, M. Amrhar, and M. Charroud (2004), A restatement of the Mesozoic Atlasic Rifting (Morocco), *J. Afr. Earth Sci.*, *38*, 145–153.
Le Roy, P., and A. Piqué (2001), Triassic-Liassic Western Moroccan synrift basins in relation to the Central Atlantic opening, *Mar. Geol.*, *172*, 359–381.
Lippolt, H. J., M. Leitz, R. S. Wernicke, and B. Hagedorn (1994), (U + Th)/He dating of apatite: Experience with samples from different geochemical environments, *Chem. Geol.*, *112*, 179–191.
Makris, J., A. Demnati, and J. Klussmann (1995), Deep seismic soundings in Morocco and a crust and upper mantle model deduced from seismic and gravity data, *Ann. Geophys.*, *3*(3), 369–380.
Malusà, M. G., R. Polino, A. C. Feroni, A. Ellero, G. Ottria, L. Baidder, and G. Musumeci (2007), Post-Variscan tectonics in eastern anti-atlas (Morocco), *Terra Nova*, *19*(6), 481–489, doi:10.1111/j.1365-3121.2007.00775.x.
Manspeizer, W. (1982), Triassic-Liassic basins and climate of the Atlantic passive margins, *Geol. Rundsch.*, *71*(3), 895–917.
Mattauer, M., F. Proust, and P. Tapponnier (1972), Major strike-slip fault of Late Hercynian Age in Morocco, *Nature*, *237*(5351), 63–72.
Mattauer, M., P. Tapponnier, and F. Proust (1977), Sur les mécanismes de formation des chaînes intracontinentales. L'exemple des chaînes atlasiques du Maroc, *Bull. Soc. Geol. Fr.*, *7*(t. XI), 521–526.
Mattis, A. F. (1977), Nonmarine Triassic sedimentation, central High Atlas Mountains, Morocco, *J. Sediment. Res.*, *47*(1), 107–119.
Medina, F. (1995), Syn- and postrift evolution of the El Jadida-Agadir basin (Morocco): Constraints for the rifting model of the Central Atlantic, *Can. J. Earth Sci.*, *32*, 1273–1291.
Michard, A. (1976), Eléments de géologie marocaine, *Notes Mém. Serv. Géol. Maroc*, *252*, 1–408.
Michard, A., A. Soulaimani, C. Hoepffner, H. Ouanaimi, L. Baidder, E. C. Rjimati, and O. Saddiqi (2010), The South-Western Branch of the Variscan Belt: Evidence from Morocco, *Tectonophysics*, *492*, 1–24, doi:10.1016/j.tecto.2010.05.021.
Michard, A., H. Ibouh, and A. Charrière (2011), Syncline-topped anticlinal ridges from the High Atlas: A Moroccan conundrum, and inspiring structures from the Syrian Arc, Israel, *Terra Nova*, *23*(5), 314–323, doi:10.1111/j.1365-3121.2011.01016.x.
Missenard, Y., H. Zeyen, D. Frizon de Lamotte, P. Leturmy, C. Petit, M. Sébrier, and O. Saddiqi (2006), Crustal versus asthenospheric origin of relief of the Atlas Mountains of Morocco, *J. Geophys. Res.*, *111*, B03401, doi:10.1029/2005JB003708.
Missenard, Y., Z. Taki, D. Frizon de Lamotte, M. Benammi, M. Hafid, P. Leturmy, and M. Sébrier (2007), Tectonic styles in the Marrakesh High Atlas (Morocco): The role of heritage and mechanical stratigraphy, *J. Afr. Earth Sci.*, *48*(4), 247–266, doi:10.1016/j.jafrearsci.2007.03.007.
Missenard, Y., O. Saddiqi, J. Barbarand, P. Leturmy, G. Ruiz, F.-Z. El Haimer, and D. Frizon de Lamotte (2008), Cenozoic denudation in the Marrakech High Atlas, Morocco: Insight from apatite fission-track thermochronology, *Terra Nova*, *20*(3), 221–228, doi:10.1111/j.1365-3121.2008.00810.x.
Morel, J., E.-M. Zouine, J. Andrieux, and A. Faure-Muret (2000), Déformations néogènes et quaternaires de la bordure nord haut atlasique (Maroc): Rôle du socle et conséquences structurales, *J. Afr. Earth Sci.*, *30*(1), 119–131.
Ouanaimi, H., and J. Petit (1992), La Limite sud de la chaine hercynienne dans le Haut Atlas marocain: Reconstitution d'un saillant non deforme, *Bull. Soc. Geol. Fr.*, *163*(1), 63–72.

Oukassou, M., O. Saddiqi, J. Barbarand, S. Sebti, L. Baidder, and A. Michard (2013), Post-Variscan exhumation of the Central Anti-Atlas (Morocco) constrained by zircon and apatite fission-track thermochronology, *Terra Nova*, *25*(2), 151–159, doi:10.1111/ter.12019.

Piqué, A., and E. Laville (1996), The central Atlantic rifting: Reactivation of Palaeozoic structures?, *J. Geodyn.*, *21*(3), 235–255.

Pique, A., and A. Michard (1989), Moroccan Hercynides: A synopsis. The Paleozoic sedimentary and tectonic evolution at the northern margin of West Africa, *Am. J. Sci.*, *289*, 286–330.

Piqué, A., P. Tricart, R. Guiraud, E. Laville, S. Bouaziz, M. Amrhar, and R. A. Ouali (2002), The Mesozoic-Cenozoic Atlas belt (North Africa): An overview, *Geodin. Acta*, *15*(3), 185–208, doi:10.1080/09853111.2002.10510752.

Price, I. (1981), Provenance of the Jurassic-Cretaceous flysch, Deep Sea Drilling Project sites 370 and 416, *Initial Rep. Deep Sea Drill. Proj.*, *50*, 751–757.

Proust, F., J. P. Petit, and P. Tapponnier (1977), L'accident du Tizi n'Test et le rôle des décrochements dans la tectonique du Haut Atlas occidental (Maroc), *Bull. Soc. Geol. Fr.*, *7*(t.XI), 541–551.

Qarbous, A., F. Medina, and C. Hoepffner (2003), Le bassin de Tizi n'Test (Haut Atlas, Maroc): Exemple d'évolution d'un segment oblique au rift de l'Atlantique central au Trias, *Can. J. Earth Sci.*, *40*, 949–964, doi:10.1139/E03-029.

Qarbous, A., F. Medina, and C. Hoepffner (2008), Tectonique cassante et état de contrainte dans le bassin de Tizi n'Test (Haut Atlas, Maroc) au cours de l'inversion tertiaire, *Estud. Geol.*, *64*(1), 17–30.

Reiners, P. W. (2005), Zircon (U-Th)/He thermochronometry, in *Low-Temperature Thermochronology: Techniques, Interpretations, and Applications*, *Rev. in Mineral. and Geochem.*, vol. 58, edited by P. W. Reiners and T. A. Ehlers, pp. 151–179.

Reiners, P. W., K. A. Farley, and H. J. Hickes (2002), He diffusion and (U–Th)/He thermochronometry of zircon: Initial results from Fish Canyon Tuff and Gold Butte, *Tectonophysics*, *349*(1–4), 297–308, doi:10.1016/S0040-1951(02)00058-6.

Reiners, P. W., T. L. Spell, S. Nicolescu, and K. A. Zanetti (2004), Zircon (U-Th)/He thermochronometry: He diffusion and comparisons with 40Ar/39Ar dating, *Geochim. Cosmochim. Acta*, *68*(8), 1857–1887, doi:10.1016/j.gca.2003.10.021.

Roch, E. (1939), Description géologique des montagnes a l'Est de Marrakech, *Notes Mém. Serv. Géol. Maroc*, *80*, 1–438.

Ruiz, G. M. H., S. Sebti, F. Negro, O. Saddiqi, D. Frizon De Lamotte, D. Stockli, J. Foeken, F. Stuart, J. Barbarand, and J. P. Schaer (2011), From central Atlantic continental rift to Neogene uplift-western Anti-Atlas (Morocco), *Terra Nova*, *23*(1), 35–41, doi:10.1111/j.1365-3121.2010.00980.x.

Saddiqi, O., F. Z. El Haimer, A. Michard, J. Barbarand, G. M. H. Ruiz, E. M. Mansour, P. Leturmy, and D. Frizon de Lamotte (2009), Apatite fission-track analyses on basement granites from south-western Meseta, Morocco: Paleogeographic implications and interpretation of AFT age discrepancies, *Tectonophysics*, *475*(1), 29–37, doi:10.1016/j.tecto.2009.01.007.

Sahabi, M., D. Aslanian, and J.-L. Olivet (2004), Un nouveau point de départ pour l'histoire de l'Atlantique central, *C. R. Geosci.*, *336*, 1041–1052.

Saura, E., et al. (2014), Syn- to post-rift diapirism and minibasins of the Central High Atlas (Morocco): The changing face of a mountain belt, *J. Geol. Soc.*, *171*(1), 97–105, doi:10.1144/jgs2013-079.

Sebti, S. (2011), Mouvements verticaux de l'Anti-Atlas occidental marocain (Kerdous et ifni): Thermochronologie par traces de fission, PhD Thesis, Univ. Hassan II of Casablanca, Morocco.

Sebti, S., O. Saddiqi, F. Z. El Haimer, A. Michard, G. Ruiz, R. Bousquet, L. Baidder, and D. Frizon de Lamotte (2009), Vertical movements at the fringe of the West African Craton: First zircon fission track datings from the Anti-Atlas Precambrian basement, Morocco, *C. R. Geosci.*, *341*(1), 71–77, doi:10.1016/j.crte.2008.11.006.

Sehrt, M. (2014), Variscan to neogene long-term landscap eevolution at the Moroccan passive continental margin (Tarfaya Basin and western anti-Atlas), PhD Thesis, Heidelberg.

Stets, J. (1992), Mid-Jurassic events in the Western High Atlas (Morocco), *Geol. Rundsch.*, *81*(1), 69–84, doi:10.1007/BF01764540.

Tari, G., and H. Jabour (2013), Salt tectonics in the Atlantic margin of Morocco, *Geol. Soc. London Spec. Publ.*, *369*, 337–353.

Tari, G., J. Molnar, and P. Ashton (2003), Examples of salt tectonics from West Africa: A comparative approach, *Geol. Soc. London Spec. Publ.*, *207*, 85–104, doi:10.1144/gsl.sp.2003.207.5.

Teixell, A., M. L. Arboleya, and M. Julivert (2003), Tectonic shortening and topography in the central High Atlas (Morocco), *Tectonics*, *22*(5), 1051, doi:10.1029/2002TC001460.

Teixell, A., P. Ayarza, H. Zeyen, M. Fernandez, and M.-L. Arboleya (2005), Effects of mantle upwelling in a compressional setting: The Atlas Mountains of Morocco, *Terra Nova*, *17*(5), 456–461, doi:10.1111/j.1365-3121.2005.00633.x.

Tesón, E. (2009), Estructura y cronología de la deformación en el borde sur del Alto Atlas de Marruecos a partir del registro tectono-sedimentario de la cuenca de antepaís de Ouarzazate, 217 pp., Univ. Autònoma de Barcelona, Barcelona, Spain.

Tesón, E., and A. Teixell (2008), Sequence of thrusting and syntectonic sedimentation in the eastern Sub-Atlas thrust belt (Dadès and Mgoun valleys, Morocco), *Int. J. Earth Sci.*, *97*(1), 103–113, doi:10.1007/s00531-006-0151-1.

Tesón, E., E. L. Pueyo, A. Teixell, A. Barnolas, J. Agustí, and M. Furió (2010), Magnetostratigraphy of the Ouarzazate Basin: Implications for the timing of deformation and mountain building in the High Atlas Mountains of Morocco, *Geodin. Acta*, *23*(4), 151–165, doi:10.3166/ga.23.151-165.

Thomas, R. J., et al. (2002), Precambrian evolution of the Sirwa window, anti-Atlas orogen, Morocco, *Precambrian Res.*, *118*, 1–57.

Van Den Bosch, J. W. H. (1971), *Carte Gravimetrique du Maroc, Scale 1:500.000*, *Notes et Mém. 234*, Ed. du Serv. Géol. du Maroc, Rabat.

Wolf, R. A., K. A. Farley, and L. T. Silver (1996), Helium diffusion and low-temperature thermochronometry of apatite, *Geochim. Cosmochim. Acta*, *60*(21), 4231–4240.

Wolfe, M. R., and D. F. Stockli (2010), Zircon (U–Th)/He thermochronometry in the KTB drill hole, Germany, and its implications for bulk He diffusion kinetics in zircon, *Earth Planet. Sci. Lett.*, *295*(1–2), 69–82, doi:10.1016/j.epsl.2010.03.025.

Zeitler, P. K., A. L. Herczig, I. McDougall, and M. Honda (1987), U-Th-He dating of apatite: A potential thermochronometer, *Geochim. Cosmochim. Acta*, *51*, 2865–2868.